



Executive summary

Characteristic stress intensity factor correlations of fatigue crack growth in high strength alloys: reviews and completion of NLR investigations 1985-1990

Problem area

For some kinds of variable amplitude (VA) fatigue load history the crack growth rates can be correlated by characteristic values of the stress intensity factor, K . Then it may be possible to estimate VA fatigue crack growth lives very efficiently by using a factor or simple equation applied to constant amplitude (CA) crack growth data. However, there are several limitations on doing this.

Description

In the period 1985 – 1990 the NLR used simple VA block programme loading to investigate characteristic- K correlations of fatigue crack growth in high strength alloys. Some of the results were published but a later investigation was not completed. This report reviews the published investigations and completes the later investigation, followed by a concluding discussion of the major points arising from the investigations.

Good characteristic- K correlations of long/large fatigue crack growth were obtainable except in the near-threshold crack growth region. Lack of correlations in this region is the consequence of fatigue crack growth curve transitions, which occur under both CA and VA loading. Transitions under VA loading occur at lower average ΔK values than those under CA loading, and VA crack growth can occur at ΔK values below the CA threshold values. Thus CA fatigue crack growth thresholds should not be used as criteria for determining whether long/large fatigue crack growth can occur under VA loading. Furthermore, it appears that fatigue crack growth thresholds are largely irrelevant for short/small \rightarrow long/large fatigue crack growth, whatever the load history. The use of CA or VA long/large fatigue crack growth threshold and near-threshold data in models for predicting fatigue crack growth could lead to (very) unconservative results.

Report no.

NLR-TP-2009-256

Author(s)

R.J.H. Wanhill

Report classification

UNCLASSIFIED

Date

September 2009

Knowledge area(s)

Aircraft Material & Damage
Research
Aerospace Materials

Descriptor(s)

fatigue
crack growth
spectrum loading

UNCLASSIFIED

Characteristic stress intensity factor correlations of fatigue crack growth in high strength alloys: reviews and completion of NLR investigations 1985-1990

Nationaal Lucht- en Ruimtevaartlaboratorium, National Aerospace Laboratory NLR

Anthony Fokkerweg 2, 1059 CM Amsterdam,
P.O. Box 90502, 1006 BM Amsterdam, The Netherlands
Telephone +31 20 511 31 13, Fax +31 20 511 32 10, Web site: www.nlr.nl

UNCLASSIFIED



NLR-TP-2009-256


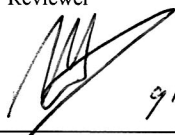

Characteristic stress intensity factor correlations of fatigue crack growth in high strength alloys: reviews and completion of NLR investigations 1985-1990

R.J.H. Wanhill

The contents of this report may be cited on condition that full credit is given to NLR and the author.
This publication has been refereed by the Advisory Committee AEROSPACE VEHICLES.

Customer National Aerospace Laboratory NLR
Contract number ----
Owner National Aerospace Laboratory NLR
Division NLR Aerospace Vehicles
Distribution Unlimited
Classification of title Unclassified
January 2010

Approved by:

Author	Reviewer	Managing department
 9/1/10	 9/1/2010	 9/1/10



Summary

For some kinds of variable amplitude (VA) fatigue load history the crack growth rates can be correlated by characteristic values of the stress intensity factor, K . Then it may be possible to estimate VA fatigue crack growth lives very efficiently by using a factor or simple equation applied to constant amplitude (CA) crack growth data. However, there are several limitations on doing this.

In the period 1985 –1990 the NLR used simple VA block programme loading to investigate characteristic- K correlations of fatigue crack growth in high strength alloys. Some of the results were published but a later investigation was not completed. This report reviews the published investigations and completes the later investigation, followed by a concluding discussion of the major points arising from the investigations.

Good characteristic- K correlations of long/large fatigue crack growth were obtainable except in the near-threshold crack growth region. Lack of correlations in this region is the consequence of fatigue crack growth curve transitions, which occur under both CA and VA loading. Transitions under VA loading occur at lower average ΔK values than those under CA loading, and VA crack growth can occur at ΔK values below the CA threshold values. Thus CA fatigue crack growth thresholds should not be used as criteria for determining whether long/large fatigue crack growth can occur under VA loading. Furthermore, it appears that fatigue crack growth thresholds are largely irrelevant for short/small \rightarrow long/large fatigue crack growth, whatever the load history. The use of CA or VA long/large fatigue crack growth threshold and near-threshold data in models for predicting fatigue crack growth could lead to (very) unconservative results.

Contents

1	Introduction	9
2	Reviews of NLR investigations 1985 – 1990: background and scope	10
3	Fatigue crack growth in landing gear steels (Wanhill 1986)	11
3.1	Test programme	11
3.2	CA fatigue crack growth rate correlations: $\log da/dN$ versus $\log \Delta K$	11
3.3	CA and block programme fatigue crack growth rate correlations: $\log da/dN$ versus $\log \Delta K_{rm}$	12
3.4	Comparison of predicted block programme a versus N curves with test data	13
4	Fatigue crack growth in 7075-T651 plate (Wanhill et al. 1986)	14
4.1	Test programme	14
4.2	Methods of characteristic-K correlation: estimates of K_{opi}	15
4.3	The NLR fatigue crack growth model CORPUS	16
4.4	CA fatigue crack growth rate correlations	17
4.5	CA and block programme fatigue crack growth rate correlations: $\log da/dN$ versus $\log \Delta K_{rm}$	18
4.6	Comparison of predicted block programme a versus N curves with test data	18
5	Low stress intensity fatigue crack growth in 4340 steel and 7475-T73 sheet	19
5.1	Test programme	19
5.2	Materials	19
5.3	Mechanical properties	20
5.4	CA and ΔK -decreasing fatigue crack growth rate correlations	20
5.4.1	Basic correlations	20
5.4.2	Low stress intensity crack opening behaviour	21
5.4.3	Crack opening models	22
5.4.4	Crack opening levels for high strength steels and aluminium alloys	22
5.4.5	CA and ΔK -decreasing $\log da/dN$ versus $\log \Delta K_{eff}$	23
5.5	CA, ΔK -decreasing and block programme fatigue crack growth rate correlations: $\log da/dN$ versus ΔK_{rm}	24
5.6	Crack growth curve transitions	24

5.6.1	CA and ΔK -decreasing loading	25
5.6.2	Block programme loading	26
6	Concluding discussion	27
6.1	Long/large fatigue crack growth	27
6.2	Short/small \rightarrow long/large fatigue crack growth	28
	References	28

Nomenclature

a	crack length
C, C'	constants in the "Paris Law"
CA	constant amplitude
CCT	centre cracked tension (specimen)
CMU	characteristic microstructural unit
CORPUS	COmputation of Retarded Propagation Under Spectrum loading
CT	compact tension (specimen)
d	dispersoid diameter
da/dN	fatigue crack growth rate
DSTO	Defence Science and Technology Organisation
K	stress intensity factor
K_{max} , $K_{max,i}$, K_{min} , $K_{min,i}$	maximum and minimum stress intensity factors
K_{op} , K_{opi}	crack opening stress intensity factor
L, T, S	longitudinal, long transverse and short transverse directions
m, m'	exponents in "Paris Law" fits
N	number of cycles or flight blocks
N_i	number of load amplitudes
N_v	number of dispersoids per unit volume
r_x , r_y , r_x^c , r_y^c	monotonic and cyclic plastic zone dimensions
R	stress ratio = S_{min}/S_{max} ; also machining radius
S	stress; also short transverse direction (see above)
S_{max} , S_{min} , S_{max1-4} , S_{min1-4} ,	maximum and minimum stresses
S_{op} , S_{op1-4}	crack opening stresses
SSCH	single side cracked hole (specimen)
T, T_1 , T_2 , T_3 , T' , T_1' , T_2' , T_3'	transitions in fatigue crack growth curves
TEM	transmission electron microscopy
UTS	ultimate tensile strength
VA	variable amplitude
α	constraint factor
Δa_i	crack length increment
ΔK	CA stress intensity factor range
ΔK_{eff}	CA effective stress intensity factor range
ΔK_i , ΔK_{imax}	VA stress intensity factor and maximum stress intensity factor ranges

ΔK_{rm}	root mean stress intensity factor range
ΔK_{th}	CA threshold stress intensity factor range
$\Delta K_{eff,th}$	CA threshold effective stress intensity factor range
λ	mean planar distance between dispersoids
σ_0	uniaxial tensile flow stress = $(\sigma_y + UTS)/2$
σ_y, σ_y^c	monotonic and cyclic yield stresses



This page is intentionally left blank.

1 Introduction

For some kinds of variable amplitude (VA) fatigue load history the crack growth rates can be correlated by characteristic values of the stress intensity factor, K . Then it may be possible to estimate VA fatigue crack growth lives very efficiently by using a factor or simple equation applied to constant amplitude (CA) crack growth data.

Such characteristic- K correlations have been tried for flight spectrum loading, with degrees of success ranging from very good to decidedly bad. This is discussed in detail in a previous NLR report (Wanhill 1994), which gave the following main conditions for successful correlations:

- (1) The spectrum is not altered by peak load clipping or load alleviation. Other changes, notably the overall severity of the spectrum, may be correlatable.
- (2) Crack growth is a regular, quasi-stationary process. This
 - Eliminates any initial transient crack growth from the fatigue “initiation” site.
 - Eliminates large differences in monotonic crack extension during peak loads.
 - Means that the peak loads are either
 - frequent and of similar magnitude, or
 - infrequent and have minor effects on crack growth rates. This is the case if the peak stresses are low and/or the constraint and material flow stress are high; and also if the basic crack growth rates are high.
- (3) The crack tip constraint and any changes in constraint, especially during peak loads, are the same.

These conditions are obviously restrictive. It was suggested that successful correlations would most likely be obtained for manoeuvre spectrum loading rather than gust spectrum loading; and for high strength alloys, which have relatively high basic crack growth rates and flow stresses. This suggestion is amply supported by recent work in the Air Vehicles Division of the Defence Science and Technology Organisation (DSTO) in Melbourne (Huynh *et al.* 2008; Molent *et al.* 2008).

2 Reviews of NLR investigations 1985 – 1990: background and scope

In the period 1985 –1990 the NLR used block programme loading representing a simplified landing gear spectrum to investigate characteristic-K correlations of fatigue crack growth in high strength alloys. Some of the results were published (Wanhill 1986; Wanhill *et al.* 1986), but a later investigation remained unreported owing to a change in priorities and discontinued funding.

During a recent discussion with DSTO colleagues it became apparent that the unreported investigation, though much simpler and less extensive than the above-mentioned DSTO work, might offer some additional insights into characteristic-K correlations. In particular, the data could be used, as was originally intended, to check the hypothesis that very low CA crack growth rates and the CA threshold stress intensity factor range, ΔK_{th} , should *not* be used to predict early or slow crack growth under VA load histories (Wanhill 1986).

This report first reviews the completed and published investigations (Wanhill 1986; Wanhill *et al.* 1986), followed by a review and completion of the later investigation. The final part of the report is a concluding discussion of the major points arising from the investigations.

3 Fatigue crack growth in landing gear steels (Wanhill 1986)

3.1 Test programme

Table 1 summarises the test programme. The environmental aspects and fractographic and metallographic correlations will not be discussed here.

Table 1 Test programme for landing gear steels

• Materials	D6AC, 4330V, 300M steel landing gear forgings
• Specimens	Standard compact tension (CT), 10 mm thick
• Fatigue loadings	<ol style="list-style-type: none"> 1. CA, R = 0.1, 66-150 Hz 2. Block programme flight-by-flight, 25 Hz
• Environments	<ol style="list-style-type: none"> 1. Fatigue in laboratory air 2. Outdoor exposure of fracture surfaces
• Examination	Fractography and metallography
• Objectives	<ol style="list-style-type: none"> 1. Characterization of fatigue and overload fractures 2. Influence of exposure on fracture surface appearances 3. Fractographic and metallographic correlations 4. Detection of flight-by-flight fracture surface markings 5. Characteristic-K correlations: 1 method 6. Comparison of predicted flight-by-flight a <i>versus</i> N curves with test data

The CT specimens were machined before being heat treated into the following ranges of ultimate tensile strength (UTS): D6AC and 4330V 1517-1655 MPa; 300M 1860-1931 MPa.

Figure 1 illustrates the block programme flight-by-flight loading. This is a simplified version of the landing gear load histories developed by Dill and Saff (1978) and Saff (1980).

3.2 CA fatigue crack growth rate correlations: $\log da/dN$ versus $\log \Delta K$

The CA fatigue crack growth rate data are compared in figure 2 with data envelopes for many steels in two ranges of yield strength (Wanhill 1978). The data points fall within the lower envelope and there was little difference between the steels. For D6AC and 4330V this is not surprising, since their nominal yield strengths were in the range 1300-1350 MPa. However, for

300M the nominal yield strength was at least 1600 MPa, so that significantly higher crack growth rates would have been expected.

The data are well represented by the “Paris Law” with the parameters given in table 2. The values of m are particularly significant: $m \leq 3$ implies good fracture toughness and the absence of monotonic tensile fracture during fatigue crack growth (Ritchie and Knott 1973).

Table 2 “Paris Law” parameters for the CA fatigue crack growth rate data

For R = 0.1, $da/dN = C(\Delta K)^m$		
Steel	C	m
D6AC	7.18×10^{-12}	2.86
4330V	5.49×10^{-11}	2.20
300M	2.46×10^{-11}	2.55

3.3 CA and block programme fatigue crack growth rate correlations: $\log da/dN$ versus $\log \Delta K_{rm}$

Root mean (rm) ΔK values were used to correlate the CA and block programme crack growth rate data. The general expression for ΔK_{rm} is

$$\Delta K_{rm} = \sqrt[m']{\frac{\sum (\Delta K_i)^{m'} N_i}{\sum N_i}} \quad [1]$$

where N_i is the number of load excursions corresponding to ΔK_i ; m' is the slope of the constant amplitude $\log da/dN$ versus $\log \Delta K_{eff}$ plot; and ΔK_i is derived from estimates of K_{opi} and the following equations:

$$(\Delta K_i)^{m'} = (K_{maxi} - K_{opi})^{m'} \quad \text{for } K_{opi} \geq K_{mini} \quad [2]$$

Equation [2] was derived by De Koning (1984). Note also that for CA loading $\Delta K_i = \Delta K_{eff} = \Delta K_{rm}$.

Estimates of K_{opi} and ΔK_{rm} were obtained as follows:

(1) CA loading, R = 0.1.

- $K_{opi} = 0.19 K_{maxi}$ (Glinka *et al.* 1984).
- $\Delta K_{rm} = K_{maxi} - K_{opi} = 0.81 K_{maxi} = 0.9 \Delta K$: this means also that $m = m'$.

- (2) Block programme loading. K_{opi} was obtained from comparisons of calculated relative spacings of fatigue striations using equation [2] and fractographic measurements. In theory this can be done in two ways:
- Assume K_{opi} to be constant during the flight block. Choose several hypothetical K_{opi} levels and calculate the relative spacings of fatigue striations in a flight block. Compare calculated and actual relative striation spacings and flight block lengths to obtain a best fit and hence an estimate of K_{opi} .
 - Assume a value of K_{opi} for one or more load excursions and derive other K_{opi} values from the actual relative spacings of fatigue striations in a flight block.

In fact, the fractographic examination, using Transmission Electron Microscopy (TEM) of two-stage replicas at magnifications up to 60,000 \times , could identify only the flight blocks and the largest striations due to the large upward load excursions in segment A of each flight block (see figure 1).

Owing to this limitation it was assumed that K_{opi} was effectively constant during each flight block and that the relative widths of the largest striations and flight blocks could be used to estimate K_{opi} . On average the largest striations accounted for slightly less than 30 % of the flight block widths. This corresponded to $K_{opi} = 0.26 K_{max}$ of each flight block. This K_{opi} value was then substituted into equations [2] to obtain ΔK_i values for each load excursion. These ΔK_i values were substituted into equation [1] to obtain ΔK_{rm} .

Figure 3 compares the block programme fatigue crack growth rate data with the CA data envelope when plotted against the derived values of ΔK_{rm} . There appears to be a very good correlation. However, subsection 3.4 shows that prediction of block programme fatigue crack growth curves using the CA data, and comparison of the predicted curves with test data, leads to a significant qualification of this “very good” correlation.

3.4 Comparison of predicted block programme a *versus* N curves with test data

Predictions of fatigue crack growth under block programme loading were done by numerically integrating “Paris Law” approximations to the CA log da/dN *versus* log ΔK_{rm} data, see table 3, and using the appropriate ΔK_{rm} values for block programme loading. The ΔK_{rm} values were derived from equations [1] and [2] using a constant K_{opi} equal to $0.26 K_{max}$ in each flight block, as in subsection 3.3.

Table 3 “Paris Law” parameters for the CA fatigue crack growth rate data correlated by ΔK_{rm}

$da/dN = C' (\Delta K)^{m'}$		
Steel	C'	m'
D6AC	9.70×10^{-12}	2.86
4330V	6.92×10^{-11}	2.20
300M	3.22×10^{-11}	2.55

Figure 4 compares the predicted *a versus N* curves with test data. The low load level results are particularly informative. Good predictions were obtained for 4330V and 300M, but the prediction for D6AC was unconservative by about 50 %. Figure 5 shows the reason: the CA “Paris Law” approximation for D6AC was a poor fit to the block programme crack growth rate data at lower ΔK_{rm} values.

In this case it would be possible to improve the predicted D6AC *a versus N* curve by adjusting the CA “Paris Law” approximation to better fit the block programme crack growth rate data. However, in practice only CA data might be available. For a best estimate the CA crack growth rate data should be obtained from as many sources as possible before fitting a “Paris Law” approximation; and even then it would seem advisable to fit an upper bound to the data to ensure conservative predictions.

4 Fatigue crack growth in 7075-T651 plate (Wanhill et al. 1986)

4.1 Test programme

Table 4 summarises the test programme. The block programme flight-by-flight loading was the same as in figure 1. Note that in this investigation there were 4 methods of obtaining characteristic-K correlations. These are discussed in subsection 4.2.

Table 4 Test programme for 7075-T651 plate

• Material	16 mm thick AA7075-T651 aluminium alloy plate
• Specimens	110 mm wide centre cracked tension (CCT) panels
• Fatigue loadings	1. CA, R = 0.1, 15 Hz 2. Block programme flight-by-flight, 15 Hz
• Environment	1. Fatigue in laboratory air
• Objectives	1. Measurement of flight-by-flight fracture surface markings 2. Characteristic-K correlations: 4 methods 3. Comparison of predicted flight-by-flight a <i>versus</i> N curves with test data

4.2 Methods of characteristic-K correlation: estimates of K_{opi}

Use of equations [1] and [2] for characteristic-K correlations requires estimates of K_{opi} . Four methods of estimating K_{opi} were employed:

- (1) Clip gauge. Numerous measurements of crack opening were made using a clip gauge mounted in central holes in the specimens. K_{opi} values were obtained by graphical treatment of load versus offset displacement data (Wanhill *et al.* 1986). This was the only method employed for CA fatigue crack growth.
- (2) CORPUS + Newman equation. The NLR fatigue crack growth model CORPUS (De Koning 1981) was used with Newman's approximate plane strain relation between S_{op}/S_{max} and R for $0 \leq R \leq 1$ (Newman 1981):

$$S_{op} = S_{max} [0.25 + 0.06R + 1.13R^2 - 0.44R^3][1 - 0.25(1 - R)^3(S_{max}/\sigma_y)^3] \quad [3]$$

where $\sigma_y = 550$ MPa for 7075-T651.

- (3) Fractography (a). Assume K_{opi} to be constant during the block programme loading. Choose several hypothetical K_{opi} levels and calculate the *relative* striation spacings using equations [2] and the proportionality

$$\Delta a_i \propto (\Delta K_i)^{m'} \quad [4]$$

Compare the calculated and actual relative striation spacings and flight block lengths to obtain a best fit and hence an estimate of K_{opi} .

- (4) Fractography (b). Assume a value of K_{opi} for one or more upward load excursions and derive other K_{opi} values from the actual relative striation spacings in a flight block and equation [2]. For this method a K_{opi}/K_{max} value of 20 % was assumed for the last four upward load excursions in part D of the flight block (see figure 1). This assumption was based on the CORPUS results in method (2).

Since two of the K_{opi} estimation methods used CORPUS, this model is discussed next.

4.3 The NLR fatigue crack growth model CORPUS

CORPUS is a cycle-by-cycle fatigue crack growth model based on approximate descriptions of crack opening behaviour that account for the magnitudes and sequence of peak loads, the growth of fatigue cracks through peak load plastic zones, and the influence of underloads (De Koning 1981). The basic features will be explained using figure 6:

- (1) Consider a fatigue crack growing under the load history in figure 6a. At the crack tip the peak load causes plastic deformation that during subsequent crack growth is assumed to result in ridges on the fracture surfaces. The height and width of these ridges depend on the magnitude of the peak load and the associated plastic zone size. The ridges are assumed to cause a local increase of the crack opening stress, S_{op} . The increase in S_{op} remains constant, for a limited amount of crack growth, until an underload occurs. The underload flattens the ridges over a distance corresponding to the *reversed* plastic zone size, thereby decreasing S_{op} , but not to the extent it was increased by the peak load. This peak load – underload effect on S_{op} is approximated in CORPUS by changing S_{op} *immediately* after a peak load or underload, as will be illustrated with figures 6b – 6j.
- (2) Figure 6b is a schematic of a load sequence consisting of several upward and downward load excursions, whereby it is assumed that fatigue crack growth occurs only during the upward load excursions.
- (3) Figure 6c shows the first pair of load excursions, to S_{max1} and S_{min1} . This sequence will *eventually* result in flattened ridges on the fracture surfaces. However, CORPUS assumes that the effect of the ridges on S_{op} occurs immediately during the next upward load excursion. The crack opening stress S_{op1} for this second upward load

excursion is obtained from analytical or empirical relations between S_{\max} , S_{\min} and S_{op} , see figure 6d.

- (3) Figure 6e adds the second upward load excursion: crack growth commences at S_{op1} and stops at $S_{\max2}$. Figure 6f adds the second downward load excursion, to $S_{\min2}$. The ridges to be formed by $S_{\max2}$ and flattened by $S_{\min2}$ will be smaller than the ridges formed by $S_{\max1}$ and will therefore have a lower crack opening stress, S_{op2} .
- (4) Figure 6g is the first illustration of load interaction effects. The third upward load excursion to $S_{\max3}$ is assumed to be effective for crack growth only above the larger of S_{op1} and S_{op2} . The mechanistic assumption is that the crack opening stress at which crack growth recommences is determined by the last ridges to lose contact.
- (5) Figure 6h is the second illustration of load interaction effects. Unloading from $S_{\max3}$ results in a minimum stress, $S_{\min3}$, below the previous ones. This will cause not only flattening of the ridges due to $S_{\max3}$, but also more flattening of the ridges due to $S_{\max1}$ and $S_{\max2}$. Thus both S_{op1} and S_{op2} will be lowered.
- (6) Figure 6i adds the next pair of load excursions, to $S_{\max4}$ and $S_{\min4}$. These illustrate two more features of CORPUS. Firstly, crack growth during the upward load excursion to $S_{\max4}$ commences at the *lowered* value of S_{op1} . Secondly, these load excursions result in a crack opening stress, S_{op4} , higher than the previous ones, the effects of which are then lost. Figure 6j adds the final upward load excursion to show that crack growth then commences at S_{op4} .

4.4 CA fatigue crack growth rate correlations

Figure 7a shows the clip gauge crack opening data plotted against ΔK . Figure 7b shows the CA crack growth rates plotted against ΔK and ΔK_{eff} ($= \Delta K_{\text{rm}}$) derived from the clip gauge data. The log da/dN versus log ΔK data can be approximated bilinearly, with the intersection point corresponding to a change in K_{op}/K_{\max} . Such changes have been observed by others (Vazquez and Morrone 1979; Kobayashi *et al.* 1981). The average K_{op}/K_{\max} lines in figure 7a were used to derive the da/dN versus ΔK_{eff} plot in figure 7b.

4.5 CA and block programme fatigue crack growth rate correlations: $\log da/dN$ versus $\log \Delta K_{rm}$

- (1) Block programme K_{opi}/K_{max} determinations. Figure 8 shows the complete set of K_{opi} determinations. The clip gauge measurements were averages from variable data obtained at five different crack lengths. These measurements were considered unreliable for estimating the contributions of individual upward load excursions to crack growth, but the average K_{opi}/K_{max} per flight block was 18.3 %. This value agreed very well with the fractographic best fit estimate in figure 8c, see figure 9 also. (However, note from figure 9 that there was a poor match between the predicted and actual striation spacings for the upward load excursions 2–5 representing parts B and C of the flight block, see figure 1).
- (2) CA and block programme correlations. Figure 10 compares the block programme fatigue crack growth data with the CA data trends when plotted against the derived values of ΔK_{rm} . The correlations were good, especially those using variable K_{opi} (methods 2 and 4), as might be expected.

4.6 Comparison of predicted block programme a versus N curves with test data

Predictions of fatigue crack growth under block programme loading were done in two ways:

- (1) Using CORPUS and equation [3], with the CA da/dN versus ΔK data as input, i.e. cycle-by-cycle crack growth calculations with variable K_{opi} .
- (2) By numerical integration of the bilinear approximation of the CA $\log da/dN$ versus $\log \Delta K_{eff}$ data and using derived ΔK_{rm} values.

Figure 11 compares the predicted a versus N curves with test data. Very good predictions were obtained from CORPUS cycle-by-cycle crack growth and numerical integration using ΔK_{rm} derived from variable K_{opi} (method 4). Reasonably conservative predictions were obtained from numerical integration using ΔK_{rm} derived from an average K_{opi}/K_{max} of 18.3% (methods 1 + 3).

These results support the CORPUS approach to estimating crack opening stresses for each upward load excursion, and also the general applicability of Newman's plane strain relation between S_{op}/S_{max} and R, equation [3]. A similar conclusion was reached by Salvetti *et al.* (1994). However, equation [3] does not account for the trend of more crack closure at lower ΔK values, see figure 7a and Vazquez and Morrone (1979) and Kobayashi *et al.* (1981).

5 Low stress intensity fatigue crack growth in 4340 steel and 7475-T73 sheet

5.1 Test programme

Table 5 summarises the test programme. The block programme flight-by-flight loading was the same as in figure 1. In this investigation there was one method of obtaining characteristic-K correlations. This is discussed in subsection 5.5.

Table 5 Test programme for 4340 steel and 7475-T73 sheet

• Materials	5.1 mm thick 4340 steel 3.5 mm thick AA7475-T73 aluminium alloy sheet
• Specimens	60 mm wide single side cracked hole (SSCH) panels
• Fatigue loadings and environment	1. CA, ΔK -decreasing; R = 0.1, 0.5; 13 Hz 2. Block programme flight-by-flight, 10 – 35 Hz 3. Laboratory air
• Other properties	1. Mechanical properties: σ_y , UTS, % elongation, σ_y^c 2. Microstructural parameters
• Objectives	1. Low stress intensity fatigue crack growth behaviour 2. Characteristic-K correlations: 1 method 3. Crack growth curve transition analyses

5.2 Materials

The 4340 steel heat treatment condition was 1 hour austenitizing at 840 °C, oil quench; 2 hours tempering at 440 °C *in vacuo*; furnace cooled in nitrogen. The microstructure consisted primarily of tempered martensite with a prior austenite grain size $\sim 10 \mu\text{m}$, and ill-defined martensite packet sizes of 2 – 10 μm see figure 12. There were occasional manganese sulphide stringers and spherical calcium aluminate inclusions (Swain *et al.* 1990). This material was supplied as 5.1 mm thick specimen blanks by the NASA Langley Research Center.

The 7475 aluminium alloy was supplied as 4 mm thick clad sheet in the T761 condition. The sheet was machined down to 3.5 mm to remove the cladding and was additionally aged to the T73 condition according to the manufacturer's recommendations (Mehr 1982). The material had

a pancake grain structure with relatively few inclusions, see figure 13. Table 6 gives details of the microstructural parameters.

Table 6 Microstructural parameters for 7475-T73 aluminium alloy sheet

Dispersoids			Subgrains (μm)	Grain dimensions (μm)
Size (μm)	Number per unit volume (μm^{-3})	Mean planar separation (μm)		
$d = 0.18 \pm 0.12$	$N_v = 36 \pm 23$	$\lambda = 0.34 \pm 0.27$	very few: 1 – 3 μm	L 232 \pm 72 T 151 \pm 32 S 26 \pm 4
$\lambda = [1.25/(N_v d)^{1/2}] - 0.82d$ (Martin 1980; Wanhill and Schra 1987)				

5.3 Mechanical properties

Table 7 gives the longitudinal mechanical properties of the materials, and figures 14 and 15 compare the monotonic and cyclic stress-strain curves for each material:

- (1) The 4340 steel was not cyclically stable. Considerable cyclic strain softening occurred, which meant that most specimens had to be tested with continuous changes in cyclic stress amplitude until failure. The hysteresis loops at about half the cyclic life were used to derive the data points for the cyclic stress-strain curve.
- (2) The 7475-T73 aluminium alloy was cyclically stable, and hence could be tested using the multiple step strain method (Landgraf *et al.* 1969). The monotonic properties met the specifications in Mehr (1982).

Table 7 Mechanical properties of the 4340 steel and 7475-T73 aluminium alloy sheet

Materials	0.2 % offset σ_y (MPa)	UTS (MPa)	Elongation on 50 mm (%)	0.2 % offset σ_y^c (MPa)
4340	1459	1511	14.5	1039
7475-T73	429	481	13.0	396

5.4 CA and ΔK -decreasing fatigue crack growth rate correlations

5.4.1 Basic correlations

The ΔK -decreasing tests were done with load shedding gradients of -0.08, i.e. following the recommendation in ASTM Standard E 647. Figures 16 – 19 show the CA and ΔK -decreasing fatigue crack growth rates with indications of the fatigue thresholds, ΔK_{th} . Figures 20 and 21 compare the crack growth rates for each material at different R values. The effect of R is less significant for 4340 steel at higher ΔK values. This was also shown by Swain *et al.* (1990).

5.4.2 Low stress intensity crack opening behaviour

Many investigations have shown that macroscopically determined K_{op} levels increase as ΔK approaches ΔK_{th} , as already indicated in figure 7b. There are two explanations for this behaviour:

- (1) Increasing fracture surface roughness, causing earlier contact of the fatigue fracture surfaces (Halliday and Beevers 1979; Suresh and Ritchie 1982).
- (2) Build-up of oxides or corrosion products on the fracture surfaces (Suresh *et al.* 1982; Vasudevan and Suresh 1982; Suresh *et al.* 1984; Wanhill and Schra 1987).

Continuum mechanics crack opening models (Newman 1981; De Koning and Liefing 1988; Nakamura and Kobayashi 1988) do not account for increasing K_{op} as ΔK_{th} is approached. Thus one may, in the first instance, question their applicability to low stress intensity fatigue crack growth. However, the reason for this discrepancy is that the models describe plasticity-induced crack opening behaviour close to the crack tip, and this behaviour, which is assumed to generally control crack growth, is unaffected by changes in fracture surface roughness or corrosion product build-up *except* at - or very close to - ΔK_{th} . Evidence for this assertion is provided by the following observations:

- For two aluminium alloys the fracture surfaces and crack wake material were machined away to within 1 mm of the tips of arrested cracks, at ΔK_{th} (Minakawa *et al.* 1983; Wanhill 1988). This machining away caused large decreases in the macroscopically measured crack opening levels, but reapplying the fatigue loading resulted in only a small amount of additional crack growth and little change in ΔK_{th} . In other words, the changes in macroscopically measured crack opening levels did not reflect the crack opening behaviour close to the crack tip.
- ΔK -decreasing tests on aluminium alloys (Vasudevan and Suresh 1983; Suresh *et al.* 1984; Wanhill *et al.* 2005) and steels (Suresh *et al.* 1981, 1982) have shown that oxide or corrosion product build-up - when it occurs, which is not always, e.g. Wanhill *et al.* (2005) - increases rapidly just before ΔK_{th} is reached. The increase in macroscopically measured crack opening levels is usually much more gradual, though there are exceptions under corrosion fatigue conditions (Wanhill and Schra 1987).

In view of the foregoing discussion, it may well be that continuum mechanics models provide better descriptions of K_{op} at low stress intensities than macroscopic measurements. This is the

motivation for using continuum mechanics models to discuss S_{op} and K_{op} behaviour in the following subsections 5.4.3 and 5.4.4.

5.4.3 Crack opening models

Newman (1981) and De Koning and Liefing (1988) developed similar crack opening models based on the Dugdale (1960) strip-yield model. These models can be used to calculate S_{op} and K_{op} as functions of R for CA loading, and hence for carefully controlled ΔK -decreasing loading. However, there is an important problem: the crack opening level depends strongly on the *constraint*, i.e. the state of stress, whether it be plane stress, plane strain or some intermediate condition.

The variations in stress state from plane stress to plane strain, and vice versa, are simulated in the models by applying a constraint factor, α , to the uniaxial tensile flow stress σ_0 . Plane stress is simulated when $\alpha = 1$, and for simulated plane strain $\alpha = 3$. These values of α are approximate lower and upper bounds derived from elastic-plastic finite element analyses of cracked bodies.

Figure 22 compares the model predictions for positive R . The De Koning and Liefing model, which is more sophisticated, predicts significantly lower crack opening levels. This is important because it demonstrates an effect of modelling capability as well as the chosen values of α .

5.4.4 Crack opening levels for high strength steels and aluminium alloys

Newman (1981, 1983), Newman and Edwards (1988), Edwards and Newman (1990), and Swain *et al.* (1990) used values of α ranging from 1 – 3 to correlate low stress intensity CA and ΔK -decreasing crack growth rate data by ΔK_{eff} . These correlations resulted in suggesting “best fit” values of $\alpha = 2.5$ for 4340 steel and $\alpha = 1.73$ for aluminium alloys (Edwards and Newman 1990).

Be that as it may, there is no “correct” value of α . This is emphasized by the fact that correlations of fatigue crack growth rate data by ΔK_{eff} can be successful when several α values are used to derive K_{op} : successful correlations require only that the choice of α and the crack opening models provide the correct *ratios* between K_{op} values for different R .

From previous work (Newman and Edwards 1988; Wanhill 1988) it seems reasonable to check the use of Newman’s model with $\alpha = 1.73$ and 3 for aluminium alloys. However, for high strength steels there is much evidence to indicate that for $0 < R < 0.4$ the S_{op}/S_{max} and K_{op}/K_{max} values lie below the $\alpha = 3$ curve (Glinka *et al.* 1984; Asami 1985; Bignonnet *et al.* 1986;

Hamano 1988). In fact, most results suggest S_{op}/S_{max} and K_{op}/K_{max} values ~ 0.19 for $R = 0.1$ (a commonly used R).

By curve fitting and optimum correlation of the 4340 steel data in figures 16, 17 and 20, two empirical crack opening equations were independently derived by Wanhill and De Koning:

$$\text{For } \alpha \sim 5.2: \quad S_{op} = S_{max} [0.175 - 0.03R + 1.9R^2 - 1.04R^3] \quad [5]$$

$$\text{For } \alpha = 6.0: \quad S_{op} = S_{max} [0.125 + 0.53R + 0.565R^2 - 0.22R^3] \quad [6]$$

These equations are for positive R and $S_{max}/\sigma_0 \leq 0.15$, as in the tests.

Figure 23 shows the S_{op}/S_{max} values derived from equations [5] and [6] together with the analytical predictions from the models of Newman (1981) and De Koning and Liefing (1988) using α values of 1.73 – 3. Note that the De Koning and Liefing model with $\alpha = 2.4$ gives the same result as Newman's model with $\alpha = 3$. The empirical equations describing the analytical predictions for $\alpha = 1.73$ and 3 can be derived from Newman (1984):

$$\text{For } \alpha = 1.73: \quad S_{op} = S_{max} [0.380 + 0.044R + 0.772R^2 - 0.196R^3] \quad [7]$$

$$\text{For } \alpha = 3: \quad S_{op} = S_{max} [0.253 + 0.030R + 1.181R^2 - 0.464R^3] \quad [8]$$

Since equations [5] and [6] give very similar results for $R \geq 0.1$, see figure 23, only equation [6] will be considered for correlating the 4340 steel data. Thus the S_{op}/S_{max} and K_{op}/K_{max} levels defined by equations [6] – [8] will be used in subsection 5.4.5 to correlate the CA and ΔK -decreasing crack growth rates by ΔK_{eff} . Later on, these equations will also be used to correlate the CA, ΔK -decreasing and block programme fatigue crack growth rates, see subsection 5.5.

5.4.5 CA and ΔK -decreasing $\log da/dN$ versus $\log \Delta K_{eff}$

- (1) 4340 steel. ΔK_{eff} values for the 4340 steel crack growth rate data were obtained from equation [6]. Correlation of the data by ΔK_{eff} is shown in figure 24. This correlation is the best obtainable. Even so, there is only a slight convergence of the crack growth curves compared to the $\log da/dN$ versus ΔK plot in figure 20. The correlation is particularly unsatisfactory in the near-threshold region.

- (2) 7475-T73. ΔK_{eff} values for the 7475-T73 aluminium alloy crack growth rate data were obtained from equations [7] and [8]. Good correlations of the data by ΔK_{eff} are shown in figure 25. A slightly better correlation is obtained for $\alpha = 1.73$, which agrees with the suggestion of Edwards and Newman (1990) to use this value of α to simulate plane strain conditions for fatigue cracks in aluminium alloys.

5.5 CA, ΔK -decreasing and block programme fatigue crack growth rate correlations: $\log da/dN$ versus ΔK_{rm}

- (1) Block programme $K_{\text{opi}}/K_{\text{max}}$ determinations. Figure 26 shows the K_{opi} determinations using equations [6] and [7] for 4340 steel and 7475-T73, respectively. Apart from cycle 1, and cycles 5 and 10 for 4340 steel, the results are very similar to those in figures 8b and 8d.
- (2) Block programme crack growth rate data. Figures 27 and 28 show the data for 4340 steel and 7475-T73 plotted against K_{max} , which was the maximum *applied* stress intensity factor at 64.3% of the maximum *in the load spectrum*, see figure 1. Note that these data were obtained under both K-increasing and K-decreasing conditions. The data for 4340 steel indicate the existence of a threshold ΔK under block programme loading.
- (3) Calculation of ΔK_{rm} . Values of ΔK_{rm} were calculated by one method, namely the use of equations [1] and [2] and the exponents $m' = 3.14$ for 4340 steel and $m' = 3.31$ for 7475-T73. These exponent values were judged to be the best fits to most of the data in figures 24 and 25. For 4340 steel $\Delta K_{\text{rm}} = 0.407 K_{\text{max}}$, and for 7475-T73 $\Delta K_{\text{rm}} = 0.341 K_{\text{max}}$, where K_{max} is defined as in (2) above*.
- (4) CA, ΔK -decreasing and block programme correlations. Figures 29 and 30 compare the block programme data with the CA and ΔK -decreasing data trends when plotted against the derived values of ΔK_{rm} . The correlations are good except in the near-threshold region. *These results are major points for the concluding discussion in section 6.*

5.6 Crack growth curve transitions

Figures 16 – 21, 24, 25, 27, 28 show that the fatigue crack growth curves obtained under CA, ΔK -decreasing and block programme loading have several “knees” or transitions. Such transitions generally occur for CA and ΔK -decreasing loading. They have been reported for

* This was also the way that K_{max} was defined in the previous investigations, though this was not explicitly stated.

high strength steels (Yoder *et al.* 1981), aluminium alloys (Yoder *et al.* 1982; Stofanak *et al.* 1983; Wanhill and Schra 1987, Wanhill 1988), titanium alloys (Irving and Beevers 1974; Yoder *et al.* 1976, 1977, 1978, 1979, 1980; Gross *et al.* 1988; Ravichandran and Dwarakadasa 1989; Wanhill *et al.* 1989; Wanhill and Looije 1993; Wang and Müller 1998), and an iron-base superalloy (Hornbogen and Zum Gahr 1976).

5.6.1 CA and ΔK -decreasing loading

Much attention has been paid to analysing the transitions observed for CA and ΔK -decreasing loading (Irving and Beevers 1974; Yoder *et al.* 1976, 1977, 1978, 1979, 1980, 1981; Gross *et al.* 1988; Ravichandran and Dwarakadasa 1989; Wanhill *et al.* 1989; Wanhill and Looije 1993; Wang and Müller 1998). It was variously concluded that the transitions occur at ΔK values where either the monotonic or cyclic plastic zone sizes at the crack tips attain and exceed the average dimensions of characteristic microstructural units (CMUs).

Figures 31 and 32 show multilinear approximations to the $\log da/dN$ versus $\log \Delta K$ plots for 4340 steel and 7475-T73, whereby the generally observed transitions are pointed out. In the present context, and in view of the block programme fatigue crack growth behaviour shown in figures 27 and 28, only the lowest transitions (T, T_1) are of interest, since these define the near-threshold crack growth regions and appear to be the most fundamental.

To analyse these transitions it is first necessary to derive the crack tip plastic zone sizes. This is particularly difficult for plane strain and cyclic loading conditions. Hahn *et al.* (1971, 1972) proposed the following dimensions of the monotonic and cyclic plastic zones directly ahead of (x-axis) and normal to (y-axis) the crack tip:

$$\text{Monotonic} \quad r_x = 0.03 (K_{\max}/\sigma_y)^2 \quad [9]$$

$$\text{plane strain} \quad r_y = 0.13 (K_{\max}/\sigma_y)^2 \quad [10]$$

$$\text{Cyclic plane} \quad r_x^c = 0.0075 (\Delta K/\sigma_y^c)^2 \quad [11]$$

$$\text{strain, } R = 0.1 \quad r_y^c = 0.033 (\Delta K/\sigma_y^c)^2 \quad [12]$$

To use equations [11] and [12] for the present data it is first necessary to convert ΔK to ΔK_{eff} . For 4340 steel this can best be done using equation [6]. This gives $\Delta K = (1.0 - 1.1)\Delta K_{\text{eff}}$. For 7475-T73 the conversion is done by using equation [7]. This gives $\Delta K = (1.2 - 1.5)\Delta K_{\text{eff}}$.

Next the approximate ΔK_{eff} and K_{\max} values at the T and T_1 transitions were estimated from figures 24 and 25 and figures 31 and 32, respectively. These values and the σ_y and σ_y^c values in

table 7 were then substituted into equations [9] – [12] to calculate the crack tip plastic zone sizes. The results are given in table 8.

Table 8 Estimates of plastic zone sizes at the T and T₁ transitions

4340 steel (T)								
R	ΔK (MPa√m)	K_{max} (MPa√m)	ΔK_{eff} (MPa√m)	$\Delta K/\Delta K_{eff}$	r_x (μm)	r_y (μm)	r_x^c (μm)	r_y^c (μm)
0.1	5.26	5.84	4.78	1.1	0.48	2.1	0.19	0.85
0.5	3.66	7.32	3.66	1.0	0.76	3.3	0.09	0.41
7475-T73 (T ₁)								
R	ΔK (MPa√m)	K_{max} (MPa√m)	ΔK_{eff} (MPa√m)	$\Delta K/\Delta K_{eff}$	r_x (μm)	r_y (μm)	r_x^c (μm)	r_y^c (μm)
0.1	2.23	2.48	1.41	1.58	1.0	4.3	0.24	1.00
0.5	1.62	3.23	0.76	2.13	1.7	7.4	0.13	0.55

From tables 7 and 8 the following possible correlations are obtained:

- At T (4340 steel) the most feasible correlation is between the martensite packet size (2 – 10 μm) and the maximum monotonic plastic zone dimension r_y (2.1 – 3.3 μm).
- At T₁ (7475-T73) the best correlations are between the dispersoid (η precipitate) spacings (0.34 ± 0.27 μm) and the cyclic plastic zone dimensions r_x^c and r_y^c (0.13 – 1.00 μm). This type of correlation agrees with previous work (Wanhill and Schra 1987; Wanhill 1988).

5.6.2 Block programme loading

Figures 33 and 34 show multilinear approximations to the log da/dN *versus* log K_{max} plots for 4340 steel and 7475-T73, pointing out the transitions T' (4340 steel) and T₂' and T₃' (7475-T73). Only the lowest transition (T' for 4340 steel) is of interest, since it defines the near-threshold crack growth region.

Analysis of the T' transition followed the same procedure as in subsection 5.6.1, using $\Delta K_{rm} = 0.407 K_{max}$ and equations [9] – [12]. The results are given in table 9.

Table 9 Estimates of plastic zone sizes at the T' transition for 4340 steel

K_{max} (MPa√m)	ΔK_{rm} (MPa√m)	r_x (μm)	r_y (μm)	r_x^c (μm)	r_y^c (μm)
7.85	3.19	0.87	3.8	0.07	0.35

From tables 7 and 9 the most feasible correlation is between the martensite packet size (2 – 10 μm) and the maximum monotonic plastic zone dimension r_y (3.8 μm). Be that as it may, the most important point is that the T' transition occurs at a lower ΔK_{rm} value (3.19 $\text{MPa}\sqrt{\text{m}}$) than the T transition (3.66 – 4.78 $\text{MPa}\sqrt{\text{m}}$), compare tables 8 and 9. *This is another major point for the concluding discussion in section 6.*

6 Concluding discussion

This section of the report is divided into two topics, *long/large* fatigue crack growth, and *short/small* \rightarrow *long/large* fatigue crack growth. This division is considered to benefit the assessment of the investigations described in sections 3 – 5. Various definitions of short/small and long/large cracks are possible (McClung *et al.* 1996), but most cracks appear to be in the long/large regime at sizes more than 0.25 – 0.5 mm (Anstee 1983; Anstee and Edwards 1983).

6.1 Long/large fatigue crack growth

All three investigations showed that good characteristic-K correlations of long/large fatigue crack growth were obtainable except in the near-threshold region. A similar result was reported for a titanium alloy (Wanhill and Looije 1993).

Lack of correlations in the near-threshold region is the consequence of fatigue crack growth curve transitions, which occur under both CA and VA loading. Transitions under VA loading occur at lower ΔK_{rm} values than those under CA loading. This was predicted already (Wanhill 1986), based on the suggestion that under increasing- ΔK conditions the transitions occur when the *cyclic* plastic zone dimensions corresponding to ΔK_{eff} or the ΔK_i due to a peak load, $\Delta K_{i\text{max}}$, exceed a particular CMU. From subsections 5.6.1 and 5.6.2 it is seen that the results for 4340 steel are more in line with the suggestion that the near-threshold transitions under CA and VA loading could occur when the *monotonic* plastic zone dimensions exceed a particular CMU, in this case the martensite packet size. However, the overall result is the same, namely that the transition T' under VA loading occurs at a lower ΔK_{rm} value (3.19 $\text{MPa}\sqrt{\text{m}}$) than the transition T under CA loading (3.66 – 4.78 $\text{MPa}\sqrt{\text{m}}$).

Not only do transitions under VA loading occur at lower ΔK_{rm} values than those under CA loading, but figures 29 and 30 provide evidence for VA crack growth at ΔK_{rm} values below the CA threshold effective stress intensity factor range, $\Delta K_{\text{eff,th}}$. Thus CA fatigue crack growth thresholds should not be used as criteria for determining whether long/large fatigue crack growth can occur under VA loading.

6.2 Short/small → long/large fatigue crack growth

The long/large fatigue crack growth results in figures 29 and 30 may be seen as limited support for the extensive test programmes of Huynh *et al.* (2008) and Molent *et al.* (2008). These investigators obtained short/small → long/large fatigue crack growth data for a high strength aluminium alloy, AA7050-T7451, tested under quasi-stationary VA block loading representing the wing load bending history for a tactical aircraft. The data showed no indications of crack growth curve transitions in the near-threshold region, as is also often the case for short/small crack growth under both CA and various realistic flight loadings (Edwards and Newman 1990; Blom 1990).

On the whole, it appears that fatigue crack growth thresholds are largely irrelevant for short/small → long/large fatigue crack growth, whatever the load history. The use of CA or VA long/large fatigue crack growth threshold and near-threshold data in models for predicting fatigue crack growth could lead to (very) unconservative results.

References

Anstee, R.F.W. (1983): An assessment of the importance of small crack growth to aircraft design, *Behaviour of Short Cracks in Aircraft Components, AGARD Conference Proceedings No. 328*, Advisory Group for Aerospace Research & Development, pp. 3-1-3-9, Neuilly-sur-Seine, France.

Anstee, R.F.W., Edwards, P.R. (1983): A review of crack growth threshold and crack propagation rates at short crack lengths, *Some Considerations on Short Crack Growth Behaviour in Aircraft Structures, AGARD Report No. 696*, Advisory Group for Aerospace Research and Development, pp. 2-1-2-12, Neuilly-sur-Seine, France.

Asami, K. (1985): Fatigue crack growth characteristic in high strength steel, *Current Research on Fatigue Cracks*, Editors T. Tanaka, M. Jono and K. Komai, The Society of Materials Science, pp. 175-199, Kyoto, Japan.

Bignonnet, A., Dias, A., Lieurade, H.P. (1986): Influence of crack closure on fatigue crack propagation, *Advances in Fracture Research (Fracture 84)*, Editors S.R. Valluri, D.M.R. Taplin, P. Rama Rao, J.F. Knott and R. Dubey, Pergamon Press, Vol. 3, pp. 1861-1868, New York, USA.

Blom, A.F. (1990): Short crack growth under realistic flight loading: model predictions and experimental results for Al 2024 and Al-Li 2090, *Short-Crack Growth Behaviour in Various*

Aircraft Materials, AGARD Report No.767, Advisory Group for Aerospace Research & Development, pp. 6-1 – 6-15, Neuilly-sur-Seine, France.

Dill, H.D., Saff, C.R. (1978): Environment–load interaction effects on crack growth, AFFDL Technical Report AFFDL-TR-78-137, Air Force Flight Dynamics Laboratory, Dayton, USA.

Dugdale, D.S. (1960): Yielding of steel sheets containing slits, *Journal of Mechanics and Physics of Solids*, Vol. 8, pp. 100-104.

Edwards, P.R., Newman, J.C., Jr. (1990): An AGARD supplemental test programme on the behaviour of short cracks under constant amplitude and aircraft spectrum loading, *Short-Crack Growth Behaviour in Various Aircraft Materials, AGARD Report No.767*, Advisory Group for Aerospace Research & Development, pp. 1-1 – 1-43, Neuilly-sur-Seine, France.

Glinka, G., Robin, C., Pluvinage, G., Chehimi, C. (1984): A cumulative model of fatigue crack growth and the crack closure effect, *International Journal of Fatigue*, Vol. 6, pp. 37-47.

Gross, T.S., Bose, S., Zhong, L. (1988): Frictional effects on fatigue crack growth in β -annealed Ti-6Al-4V, *Fatigue and Fracture of Engineering Materials and Structures*, Vol. 11, pp. 179-187.

Hahn, G.T., Sarrate, M., Rosenfield, A.R. (1971): Plastic zones in Fe-3Si steel double-cantilever-beam specimens, *International Journal of Fracture Mechanics*, Vol. 7, pp. 435-446.

Hahn, G.T., Hoagland, R.G., Rosenfield, A.R. (1972): Local yielding attending fatigue crack growth, *Metallurgical Transactions*, Vol. 3, pp. 1189-1202.

Halliday, M.D., Beevers, C.J. (1979): Non-closure of cracks and fatigue crack growth in β -heat treated Ti-6Al-4V, *International Journal of Fracture*, Vol. 15, pp. R27-R30.

Hamano, R. (1988): The effect of microstructure on the fatigue crack growth behavior of age-hardened high strength steels in a corrosive environment, *Metallurgical Transactions A*, Vol. 19A, pp. 1461-1469.

Hornbogen, E., Zum Gahr, K.H. (1976): Microstructure and fatigue crack growth in a γ -Fe-Ni-Al alloy, *Acta Metallurgica*, Vol. 24, pp. 581-592.

Huynh, J., Molent, L., Barter, S.A. (2008): Experimentally derived crack growth models for different stress concentration factors, *International Journal of Fatigue*, Vol. 30, pp. 1766-1786.

Irving, P.E., Beevers, C.J. (1974): Microstructural influences on fatigue crack growth in Ti-6Al-4V, *Materials Science and Engineering*, Vol. 14, pp.229-238.

Kobayashi, H., Nakamura, H., Nakazawa, H. (1981): Mechanics of fatigue crack growth: comparison between fatigue and ideal fatigue cracks, *Mechanics of Fatigue, AMD-Vol. 47*, Editor T. Mura, American Society of Mechanical Engineers, pp. 133-150, New York, USA.

Koning, A.U. de (1981): A simple crack closure model for prediction of fatigue crack growth rates under variable-amplitude loading, *Fracture Mechanics: Thirteenth Conference, ASTM STP 743*, Editor R. Roberts, American Society for Testing and Materials, pp. 63-85, Philadelphia, USA.

Koning, A.U. de (1984): Crack growth prediction methods, NLR Technical Report NLR TR 84121 L, National Aerospace Laboratory NLR, Amsterdam, the Netherlands.

Koning, A.U. de, Liefing, G. (1988): Analysis of crack opening behavior by application of a discretized strip yield model, *Mechanics of Fatigue Crack Closure, ASTM STP 982*, Editors J.C. Newman, Jr. and W. Elber, American Society for Testing and Materials, pp. 437-458, Philadelphia, USA.

Landgraf, R.W., Morrow, J., Endo, T. (1969): Determination of the cyclic stress-strain curve, *Journal of Materials*, Vol. 4, pp. 176-188.

Martin, J.W. (1980): *Micromechanisms in Particle-Hardened Alloys*, Cambridge University Press, Cambridge, UK.

McClung, R.C., Chan, K.S., Hudak, Jr., S.J., Davidson, D.L. (1996): Behavior of small fatigue cracks, *ASM Handbook Volume 19 Fatigue and Fracture*, Editors S.R. Lampman *et al.*, ASM International, pp. 153-158, Materials Park, USA.

Mehr, P.L. (1982): Addendum 1982 May 21 to ALCOA 7475 sheet and plate, 3rd revised issue, 1978 February, Aluminum Company of America (ALCOA) Application Engineering Division, New Kensington, USA.

Minakawa, K., Newman, J.C. Jr., McEvily, A.J. (1983): A critical study of the crack closure effect on near-threshold fatigue crack growth, *Fatigue of Engineering Materials and Structures*, Vol. 6, pp. 359-365.

Molent, L., McDonald, M., Barter, S., Jones, R. (2008): Evaluation of spectrum fatigue crack growth using variable amplitude data, *International Journal of Fatigue*, Vol. 30, pp. 119-137.

Nakamura, H., Kobayashi, H. (1988): Analysis of fatigue crack closure caused by asperities using the modified Dugdale model, *Mechanics of Fatigue Crack Closure*, ASTM STP 982, Editors J.C. Newman, Jr. and W. Elber, American Society for Testing and Materials, pp. 459-472, Philadelphia, USA.

Newman, J.C., Jr. (1981): A crack-closure model for predicting fatigue crack growth under aircraft spectrum loading, *Methods and Models for Predicting Fatigue Crack Growth Under Random Loading*, ASTM STP 748, Editors J.B. Chang and C.M. Hudson, American Society for Testing and Materials, pp. 53-84, Philadelphia, USA.

Newman, J.C., Jr. (1983): A nonlinear fracture mechanics approach to the growth of small cracks, *Behaviour of Short Cracks in Airframe Components*, AGARD Conference Proceedings no. 328, Advisory Group for Aerospace Research & Development, pp. 6-1 – 6-26, Neuilly-sur-Seine, France.

Newman, J.C., Jr. (1984): A crack opening stress equation for fatigue crack growth, *International Journal of Fracture*, Vol. 24, pp. R131-R135.

Newman, J.C., Jr., Edwards, P.R. (1988): *Short-Crack Growth Behaviour in an Aluminium Alloy – an AGARD Cooperative Test Programme*, AGARD Report No. 732, Advisory Group for Aerospace Research & Development, Neuilly-sur-Seine, France.

Ravichandran, K.S., Dwarakadasa, E.S. (1989): Fatigue crack growth transitions in Ti-6Al-4V alloy, *Scripta METALLURGICA*, Vol. 23, pp. 1685-1690.

Ritchie, R.O., Knott, J.F. (1973): Mechanisms of fatigue crack growth in low alloy steels, *Acta Metallurgica*, Vol. 21, pp. 639-648.

Saff, C.R. (1980): Environment-load interaction effects on crack growth in landing gear steels, NADC Report NADC-79095-60, Naval Air Development Center, Warminster, USA.

Salveti, A., Lazzeri, L., Pieracci, A. (1994): An assessment of fatigue crack growth prediction models for aerospace structures, *An Assessment of Fatigue Damage and Crack Growth Prediction Techniques*, AGARD Report 797, Advisory Group for Aerospace Research & Development, pp. 6-1 – 6-17, Neuilly-sur-Seine, France.

Stofanek, R.J., Hertzberg, R.W., Leupp, J., Jaccard, R. (1983): On the cyclic behavior of cast and extruded aluminum alloys. Part B: fractography, *Engineering Fracture Mechanics*, Vol. 17, pp. 541-554.

Suresh, S., Parks, D.M., Ritchie, R.O. (1982): Crack tip oxide formation and its influence on fatigue thresholds, *Fatigue Thresholds: Fundamentals and Engineering Applications*, Editors J. Bäcklund, A.F. Blom and C.J. Beevers, Engineering Materials Advisory Services Ltd., Vol. I, pp. 391-408, Warley, UK.

Suresh, S., Ritchie, R.O. (1982): A geometric model for fatigue crack closure induced by fracture surface roughness, *Metallurgical Transactions A*, Vol. 13A, pp. 1627-1631.

Suresh, S., Vasudevan, A.K., Bretz, P.E. (1984): Mechanisms of slow fatigue crack growth in high strength aluminum alloys: role of microstructure and environment, *Metallurgical Transactions A*, Vol. 15A, pp. 369-379.

Suresh, S., Zamiski, G.F., Ritchie, R.O. (1981): Oxide-induced crack closure: an explanation for near-threshold corrosion fatigue crack growth behavior, *Metallurgical Transactions A*, Vol. 12A, pp. 1435-1443.

Swain, M.H., Everett, R.A., Newman, J.C., Jr., Phillips, E.P. (1990): The growth of short cracks in 4340 steel and aluminum-lithium 2090, *Short-Crack Growth Behaviour in Various Aircraft Materials*, AGARD Report No.767, Advisory Group for Aerospace Research & Development, pp. 7-1 – 7-30, Neuilly-sur-Seine, France.

Vasudevan, A.K., Suresh, S. (1982): Influence of corrosion deposits on near-threshold fatigue crack growth behavior in 2XXX and 7XXX series aluminum alloys, *Metallurgical Transactions A*, Vol. 13A, pp. 2271-2280.

Vazquez, J.A., Morrone, A. (1979): Experimental results on fatigue crack closure for two aluminium alloys, *Engineering Fracture Mechanics*, Vol. 12, pp. 231-240.

Wang, S.-H., Müller, C. (1998): A study on the change of fatigue fracture mode in two titanium alloys, *Fatigue and Fracture of Engineering Materials and Structures*, Vol. 21, pp. 1077-1087.

Wanhill, R.J.H. (1978): Microstructural influences on fatigue and fracture resistance in high strength structural materials, *Engineering Fracture Mechanics*, Vol. 10, pp. 337-357.

Wanhill, R.J.H. (1986): Fatigue fracture in landing gear steels, *ICAS Proceedings 1986, 15th Congress of the International Council of the Aeronautical Sciences*, Editors P. Santini and R. Staufenbiel, American Institute of Aeronautics and Astronautics, Inc., Vol. 2, pp. 1347-1355, New York, USA.

Wanhill, R.J.H. (1988): Low stress intensity fatigue crack growth in 2024-T3 and T351, *Engineering Fracture Mechanics*, Vol. 30, pp. 233-260.

Wanhill, R.J.H. (1994): Damage tolerance engineering property evaluations of aerospace aluminium alloys with emphasis on fatigue crack growth, NLR Technical Publication NLR TP 94177 U, National Aerospace Laboratory NLR, Amsterdam, the Netherlands.

Wanhill, R.J.H., Galatolo, R., Looije, C.E.W. (1989): Fractographic and microstructural analysis of fatigue crack growth in a Ti-6Al-4V fan disc forging, *International Journal of Fatigue*, Vol. 11, pp. 407-416.

Wanhill, R.J.H., Looije, C.E.W. (1993): Fractographic and microstructural analysis of fatigue crack growth in Ti-6Al-4V fan disc forgings, *AGARD Engine Disc Cooperative Test Programme*, AGARD Report 766 (Addendum), Advisory Group for Aerospace Research and Development, Neuilly-sur-Seine, France, pp. 2-1-2-40.

Wanhill, R.J.H., Koning, A.U. de, Schra, L. (1986): Modelling of fatigue crack growth in 7075-T651 aluminium alloy plate, *Fracture Control of Engineering Structures – ECF 6*, Editors H.C. van Elst and A. Bakker, Engineering Materials Advisory Services Ltd., Vol. II, pp. 1243-1253, Warley, UK.

Wanhill, R.J.H., Schra, L. (1987): Corrosion fatigue crack arrest in aluminium alloys: basic data, NLR Technical Report NLR TR 87128 U, National Aerospace Laboratory NLR, Amsterdam, the Netherlands.

Wanhill, R.J.H., Ubels, L.C., Bos, M.J., Hattenberg, T. (2005): Determination of fatigue crack growth thresholds, HeliDamTol – WP4 results: part I, NLR Contract Report NLR-CR-2005-595, National Aerospace Laboratory NLR, Amsterdam, the Netherlands.

Yoder, G.R., Cooley, L.A., Crooker, T.W. (1976): A micromechanistic interpretation of cyclic crack-growth behavior in a beta-annealed Ti-6Al-4V alloy, NRL Report 8048, Naval Research Laboratory, Washington, D.C., USA.

Yoder, G.R., Cooley, L.A., Crooker, T.W. (1977): Observations on microstructurally sensitive fatigue crack growth in a Widmanstätten Ti-6Al-4V alloy, *Metallurgical Transactions A*, Vol. 8A, pp. 1737-1743.

Yoder, G.R., Cooley, L.A., Crooker, T.W. (1978): Fatigue crack propagation resistance of beta-annealed Ti-6Al-4V alloys of differing interstitial oxygen contents, *Metallurgical Transactions A*, Vol. 9A, pp. 1413-1420.



Yoder, G.R., Cooley, L.A., Crooker, T.W. (1979): 50-fold difference in Region-II fatigue crack propagation resistance of titanium alloys: a grain size effect, *Journal of Engineering Materials and Technology*, Vol. 101, pp. 86-90.

Yoder, G.R., Cooley, L.A., Crooker, T.W. (1980): Observations on the generality of the grain-size effect on fatigue crack growth in $\alpha + \beta$ titanium alloys, *Titanium '80 Science and Technology*, Editors H. Kimura and O. Izumi, The Metallurgical Society of AIME, Warrendale, USA, pp. 1865-1873.

Yoder, G.R., Cooley, L.A., Crooker, T.W. (1981): A critical analysis of grain-size and yield-strength dependence of near-threshold fatigue-crack growth in steels, NRL Memorandum Report 4576, Naval Research Laboratory, Washington, D.C., USA.

Yoder, G.R., Cooley, L.A., Crooker, T.W. (1982): On microstructural control of near-threshold fatigue crack growth in 7000-series aluminium alloys, *Scripta METALLURGICA*, Vol. 16, pp. 1021-1025.

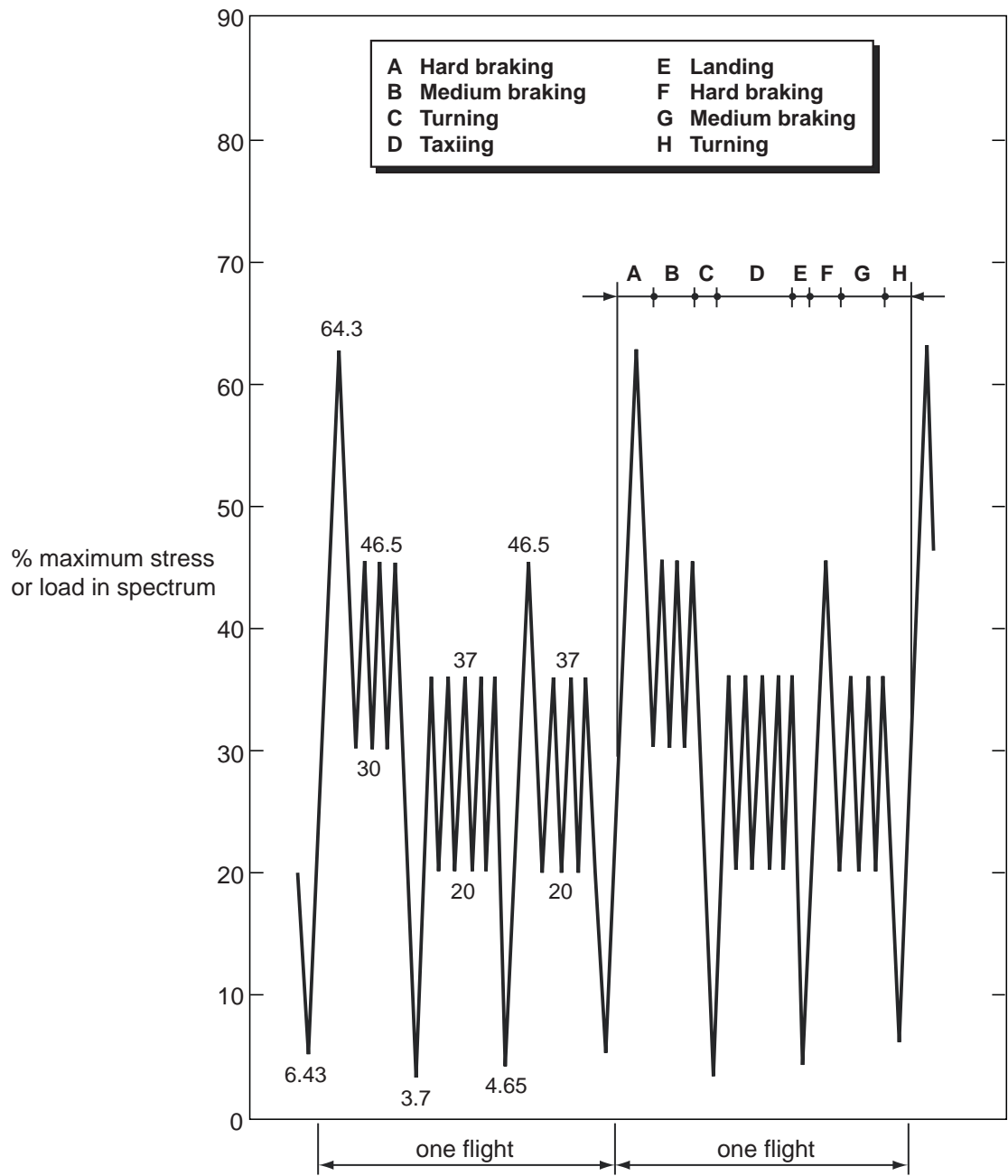


Fig. 1 Block programme flight-by-flight loading representing the load history of a tactical aircraft landing gear

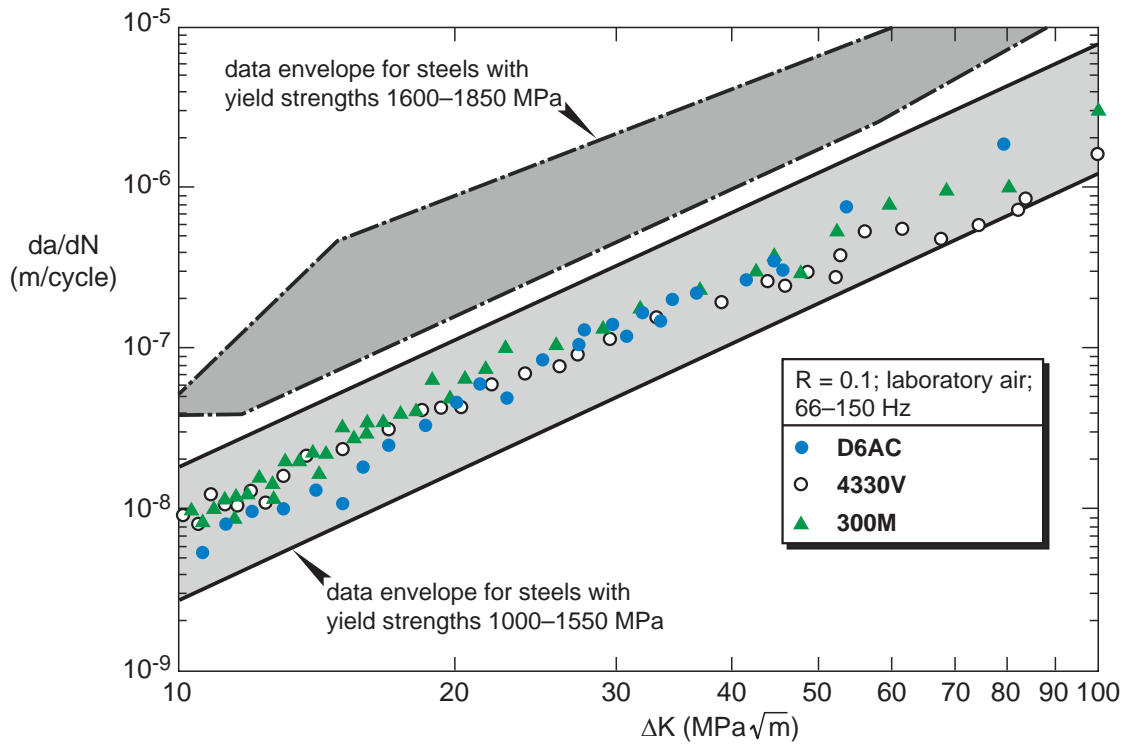


Fig. 2 CA fatigue crack growth rate data for landing gear steels (Wanhill 1986)

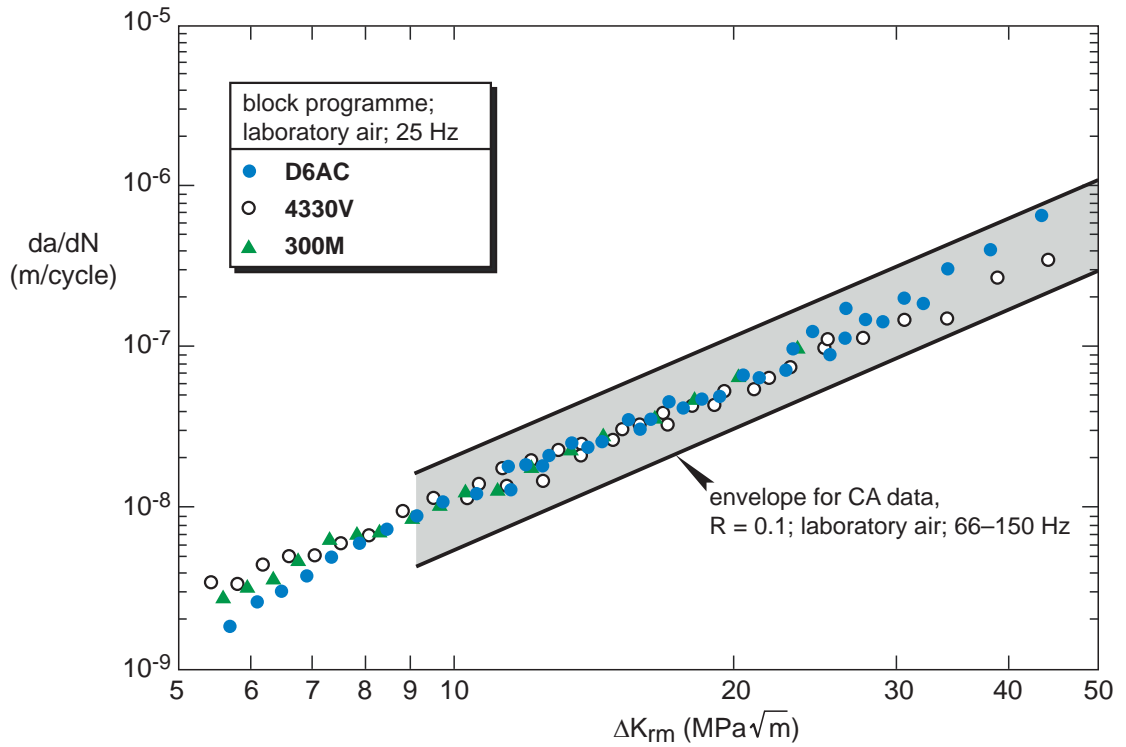


Fig. 3 Correlation of block programme and CA fatigue crack growth rate data for landing gear steels by ΔK_{rm} (Wanhill 1986)

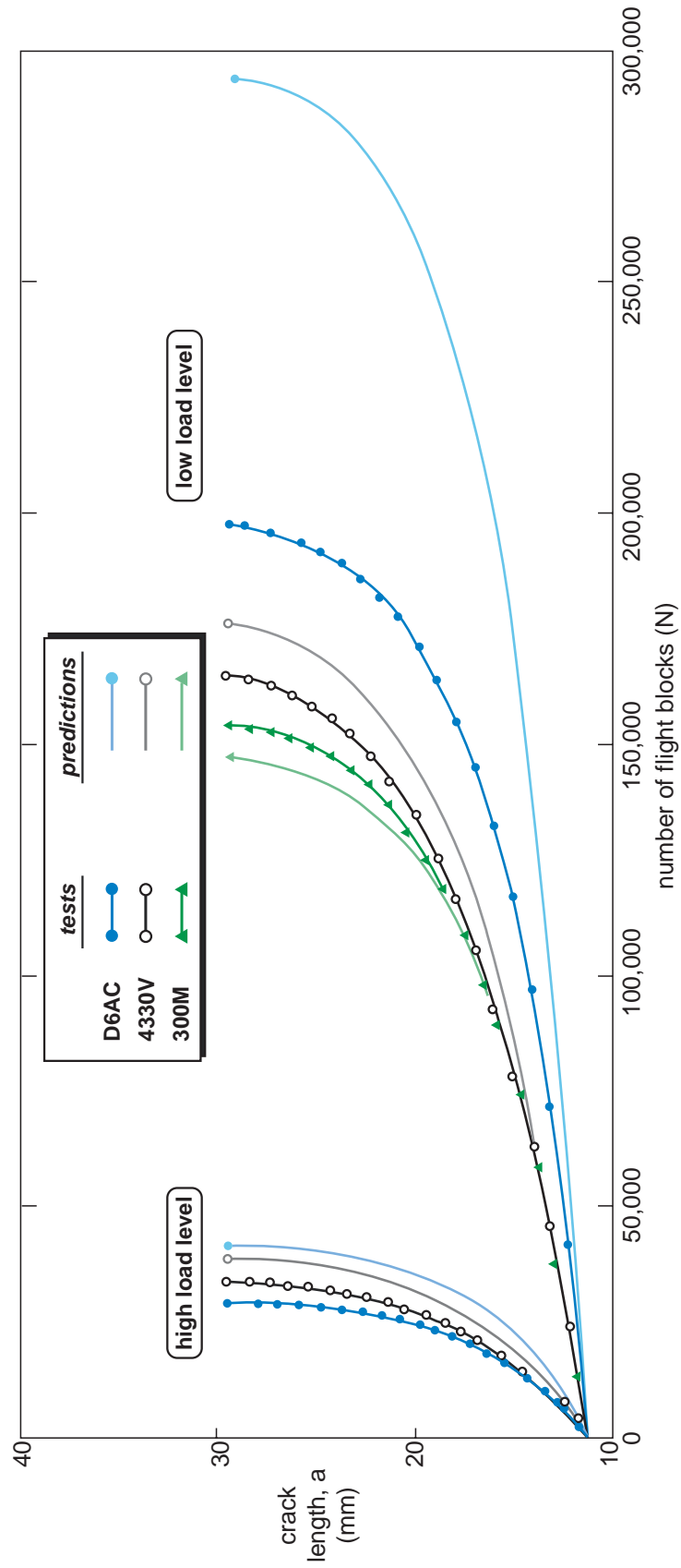


Fig. 4 Comparison of predicted block programme crack growth curves with test data (Wanhill 1986)

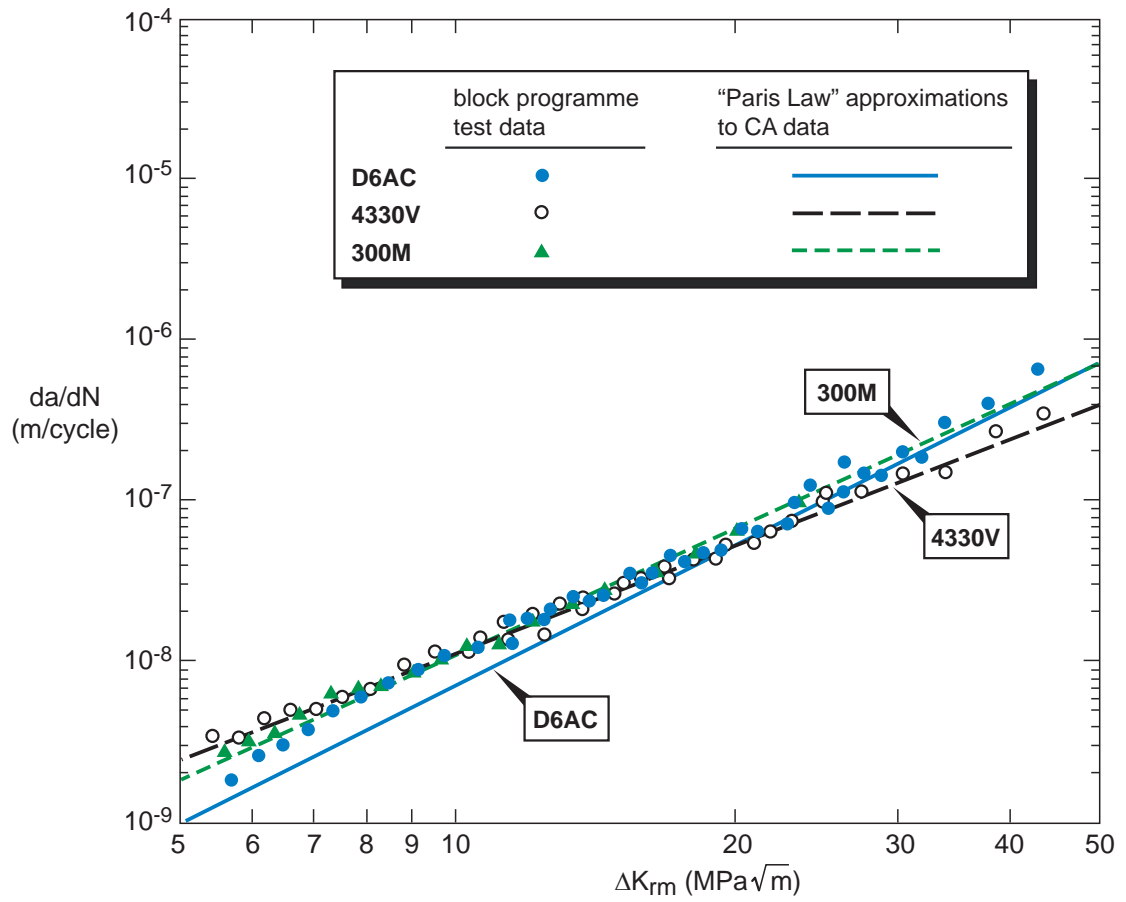


Fig. 5 Comparison of CA "Paris Law" approximations with block programme crack growth rate data (Wanhill 1986)

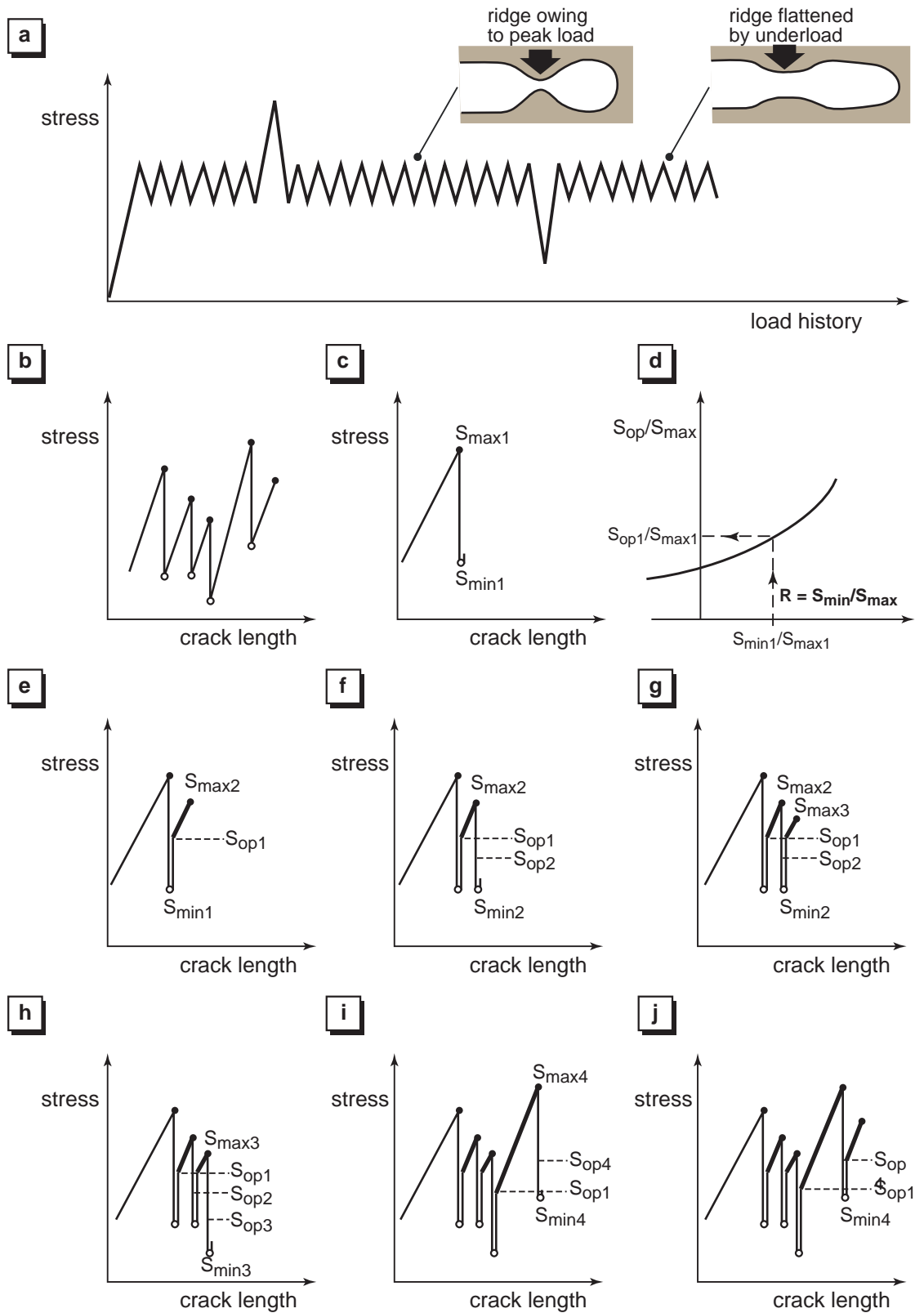


Fig. 6 Crack opening behaviour modelled in CORPUS

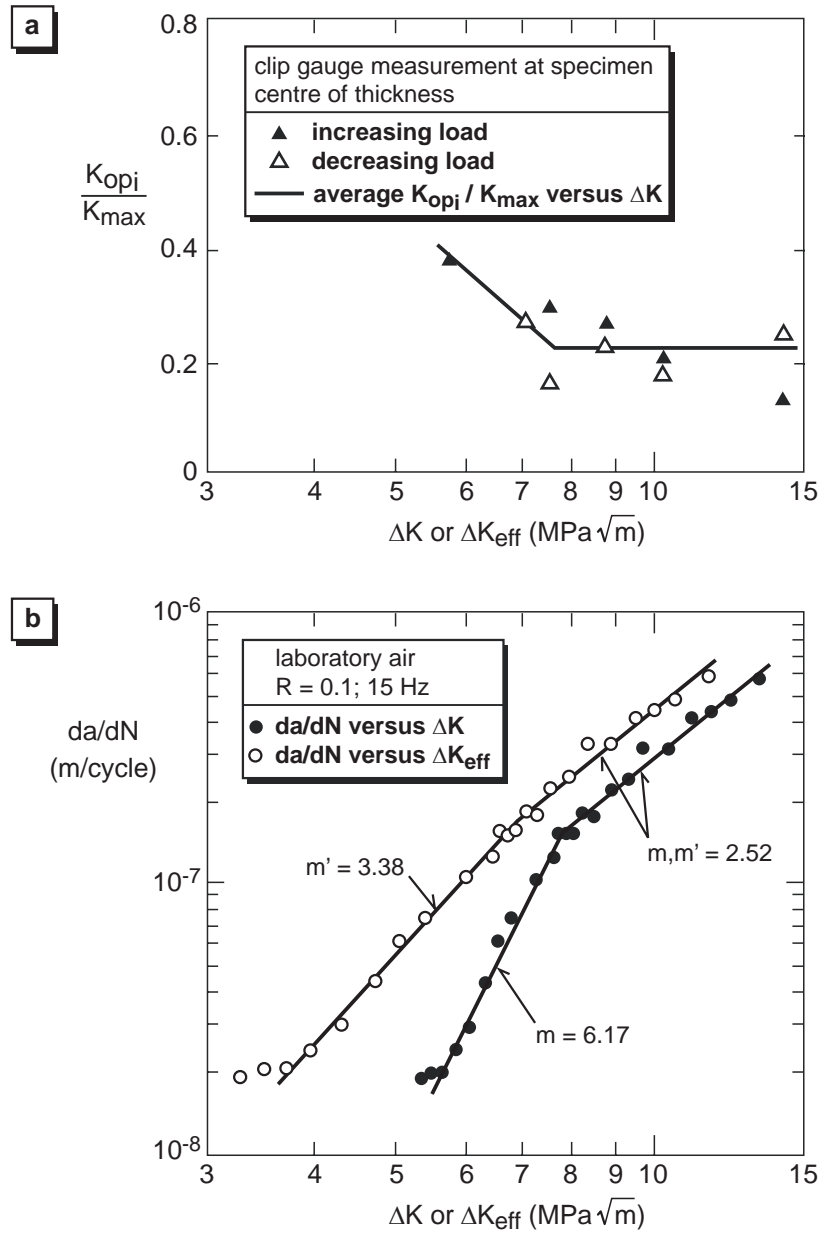


Fig. 7 CA crack growth rate data correlations by ΔK and ΔK_{eff} for 7075-T651 (Wanhill et al. 1986)

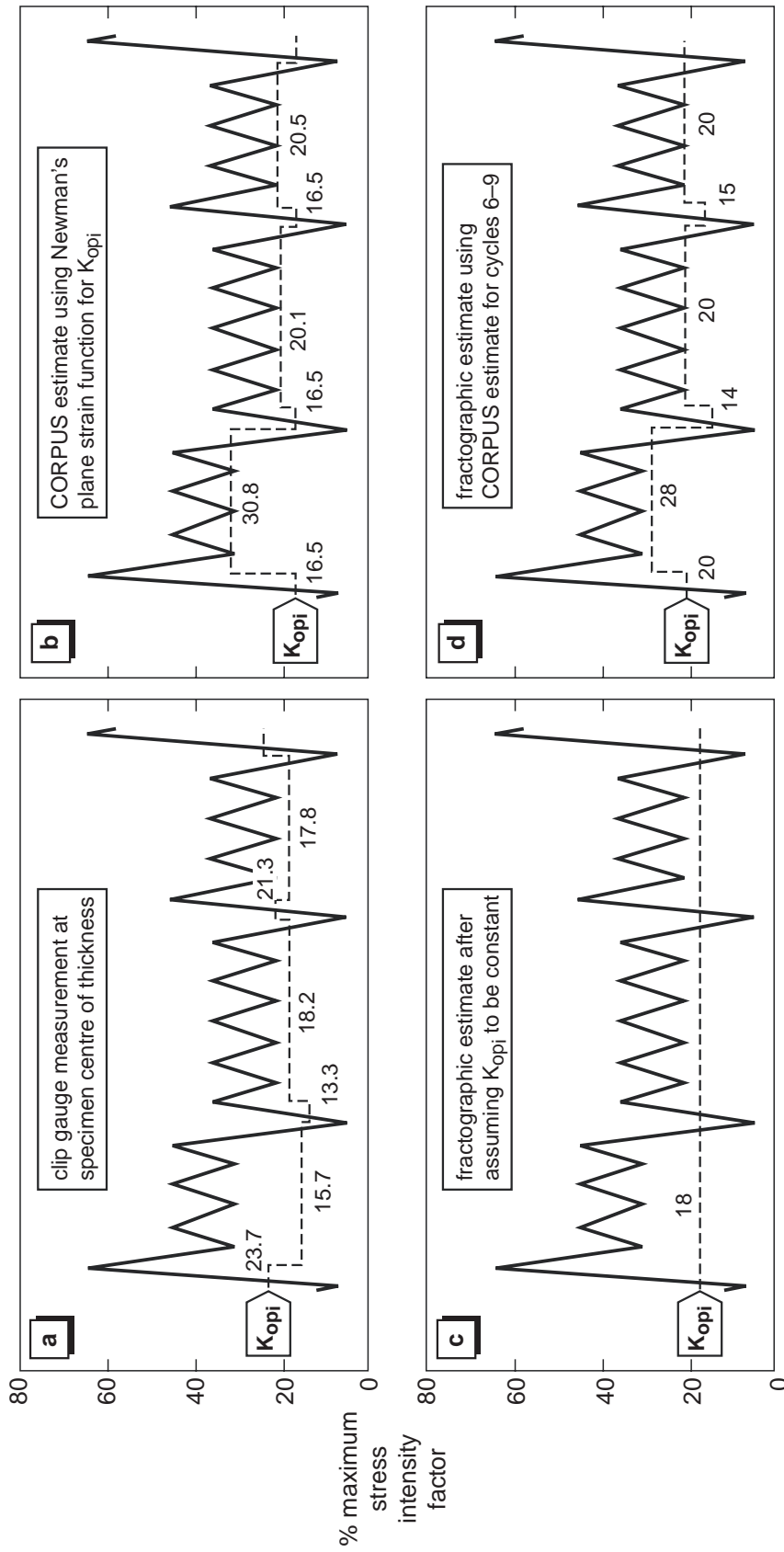


Fig. 8 Estimates of K_{opi} during a flight block (Wanhill et al. 1986). Compare with figure 26

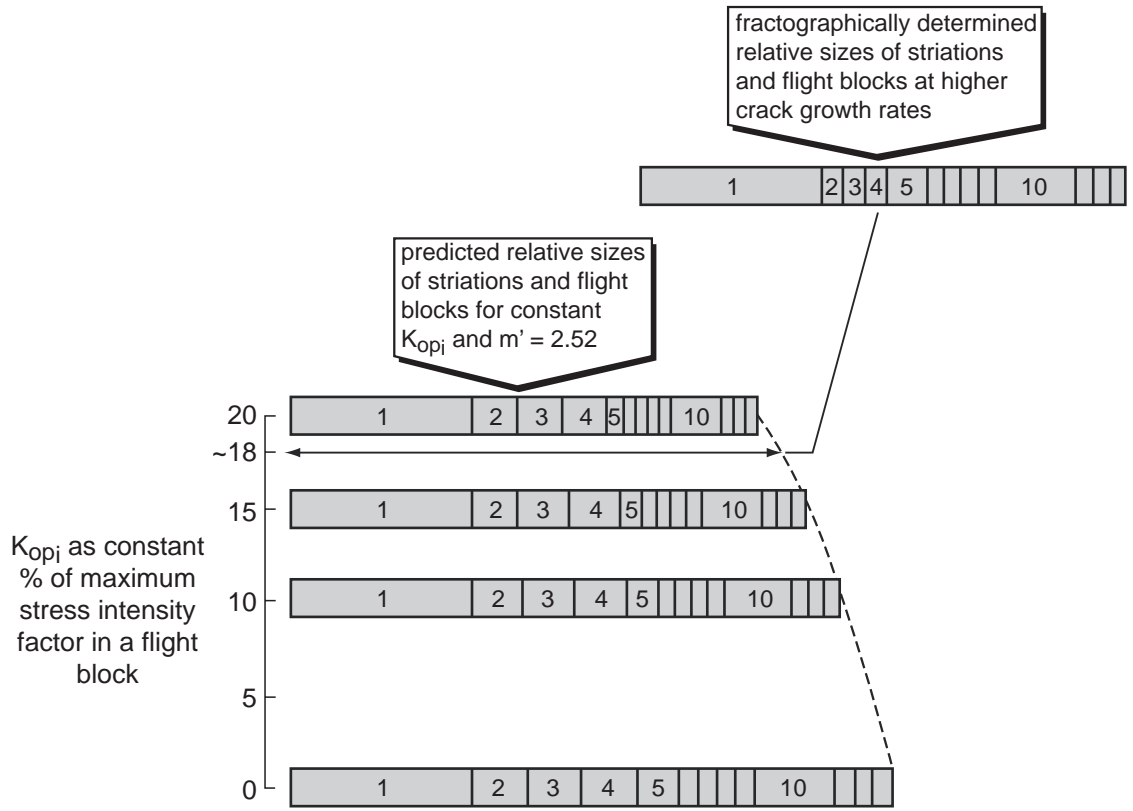


Fig. 9 Predicted and actual sizes of striations and flight blocks normalized to the largest load excursion. The best fit is with a constant $K_{Op_i} = 18\%$ of K_{max} (Wanhill et al. 1986)

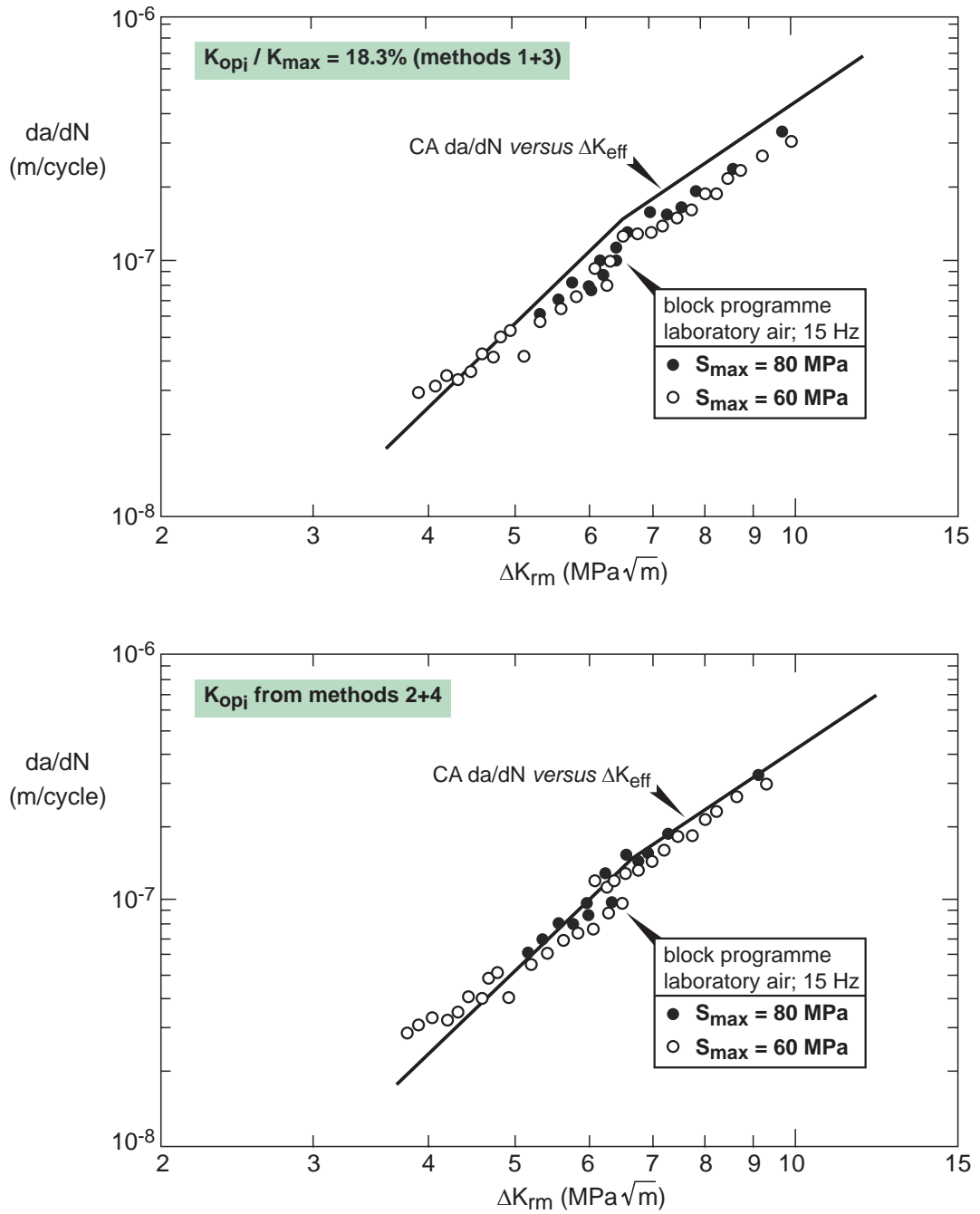


Fig. 10 Correlation of block programme and CA fatigue crack growth data for 7075-T651 by ΔK_{rm} (Wanhill et al. 1986)

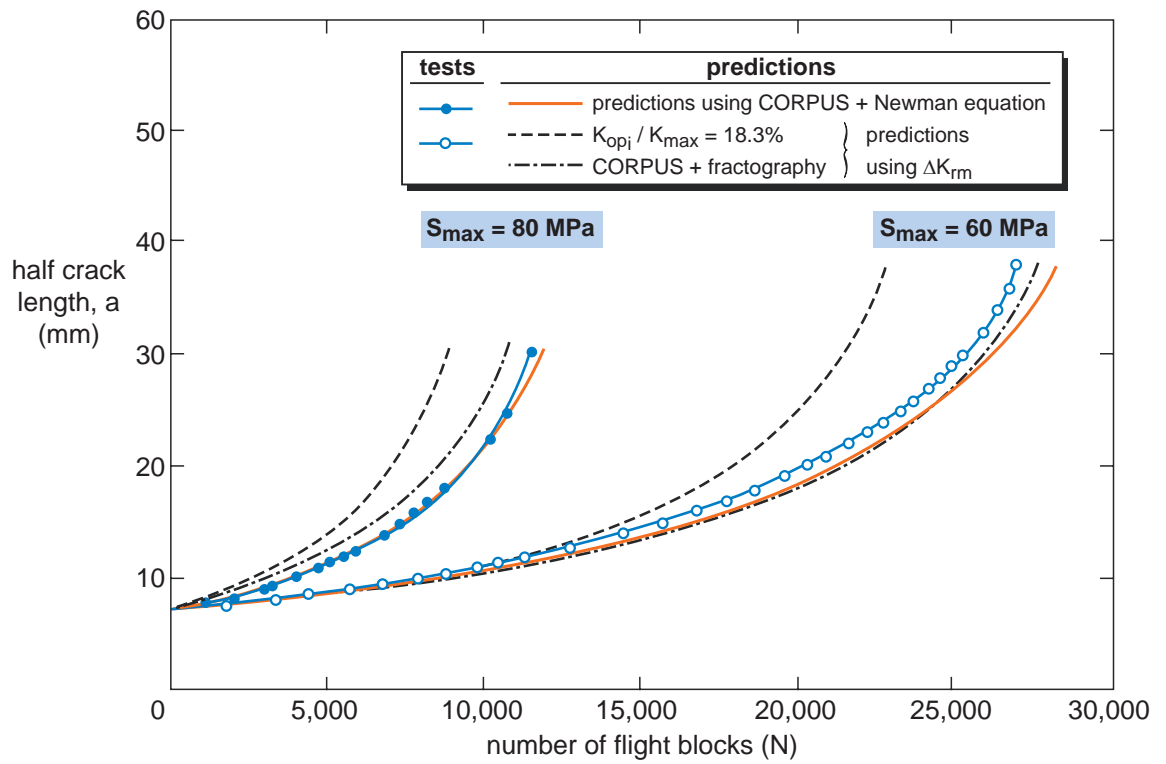


Fig. 11 Comparison of predicted block programme crack growth curves with test data (Wanhill et al. 1986)

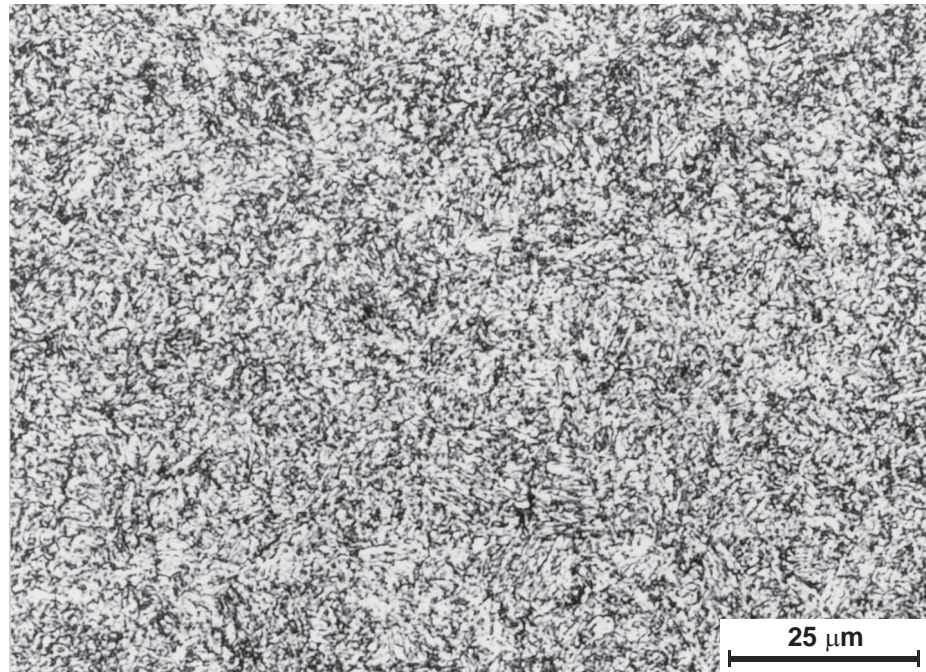


Fig. 12 Ill-defined martensite packets in the 4340 steel

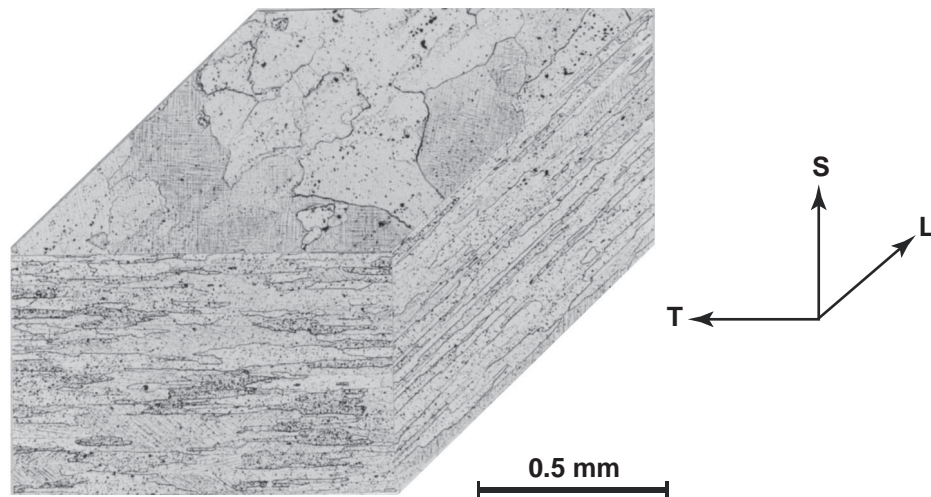


Fig. 13 Pancake grain structure of the 7475-T73 sheet

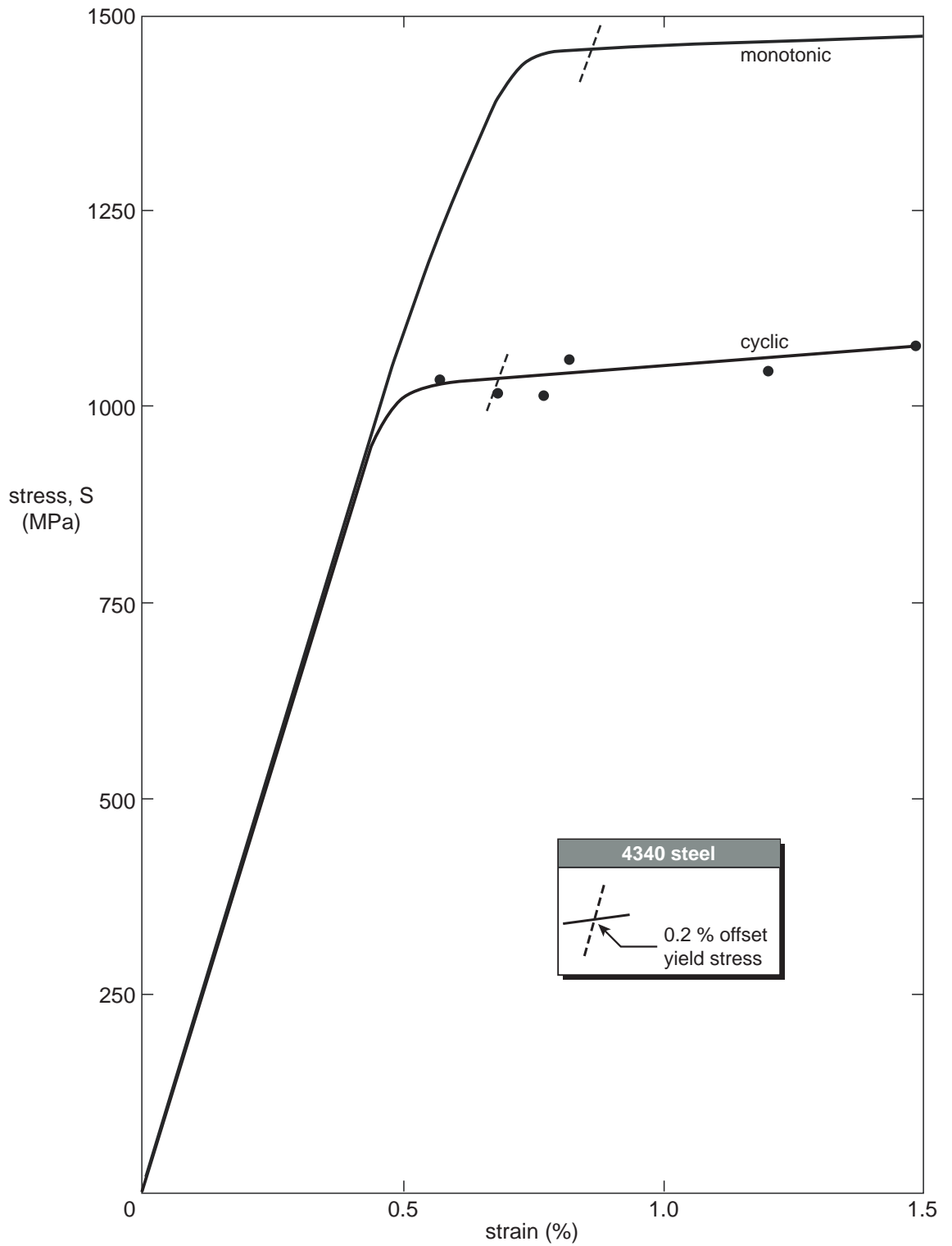


Fig. 14 Monotonic and cyclic stress-strain curves for 4340 steel. The monotonic curve is the average for three specimens

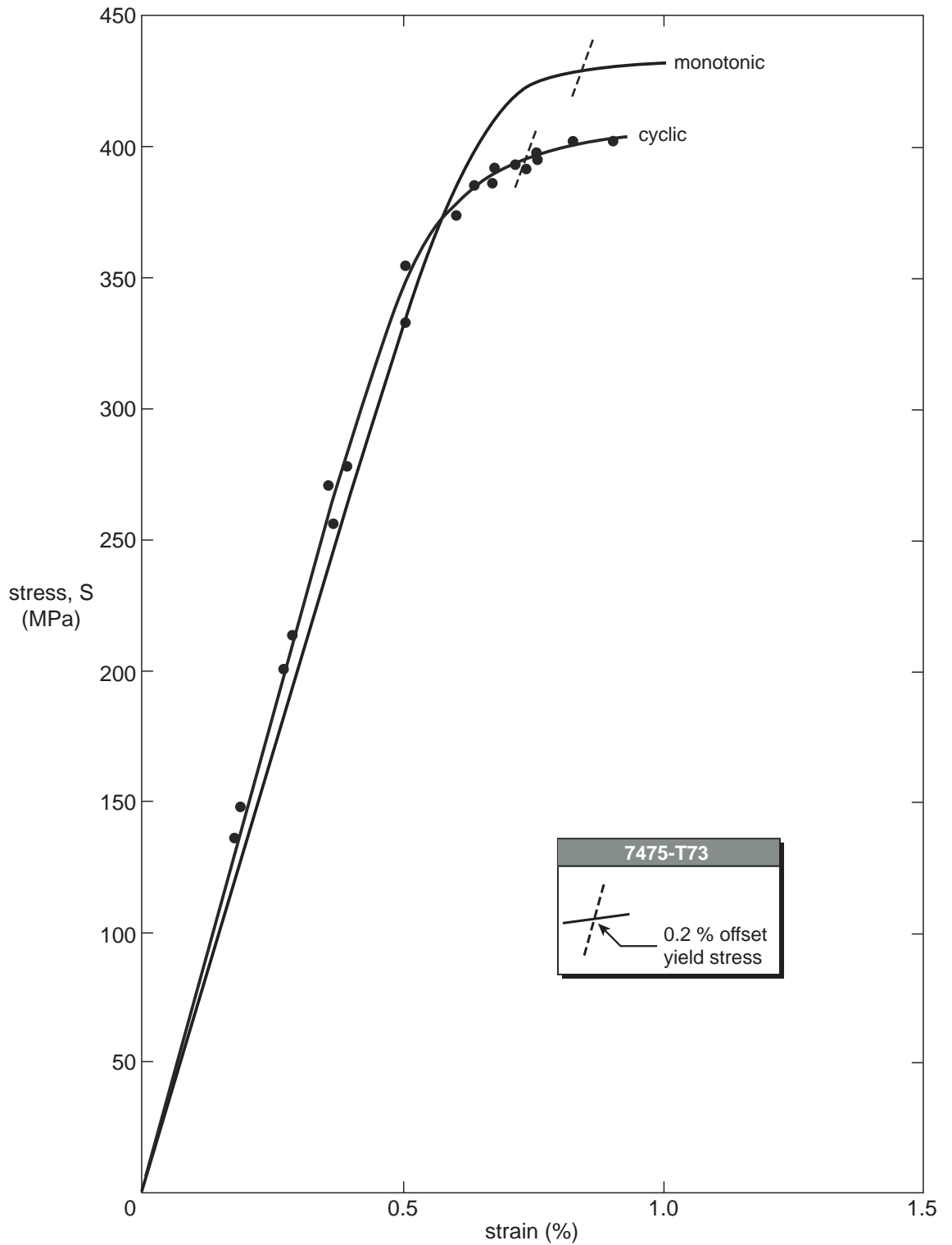


Fig. 15 Monotonic and cyclic stress-strain curves for 7475-T73. The monotonic curve is the average for three specimens

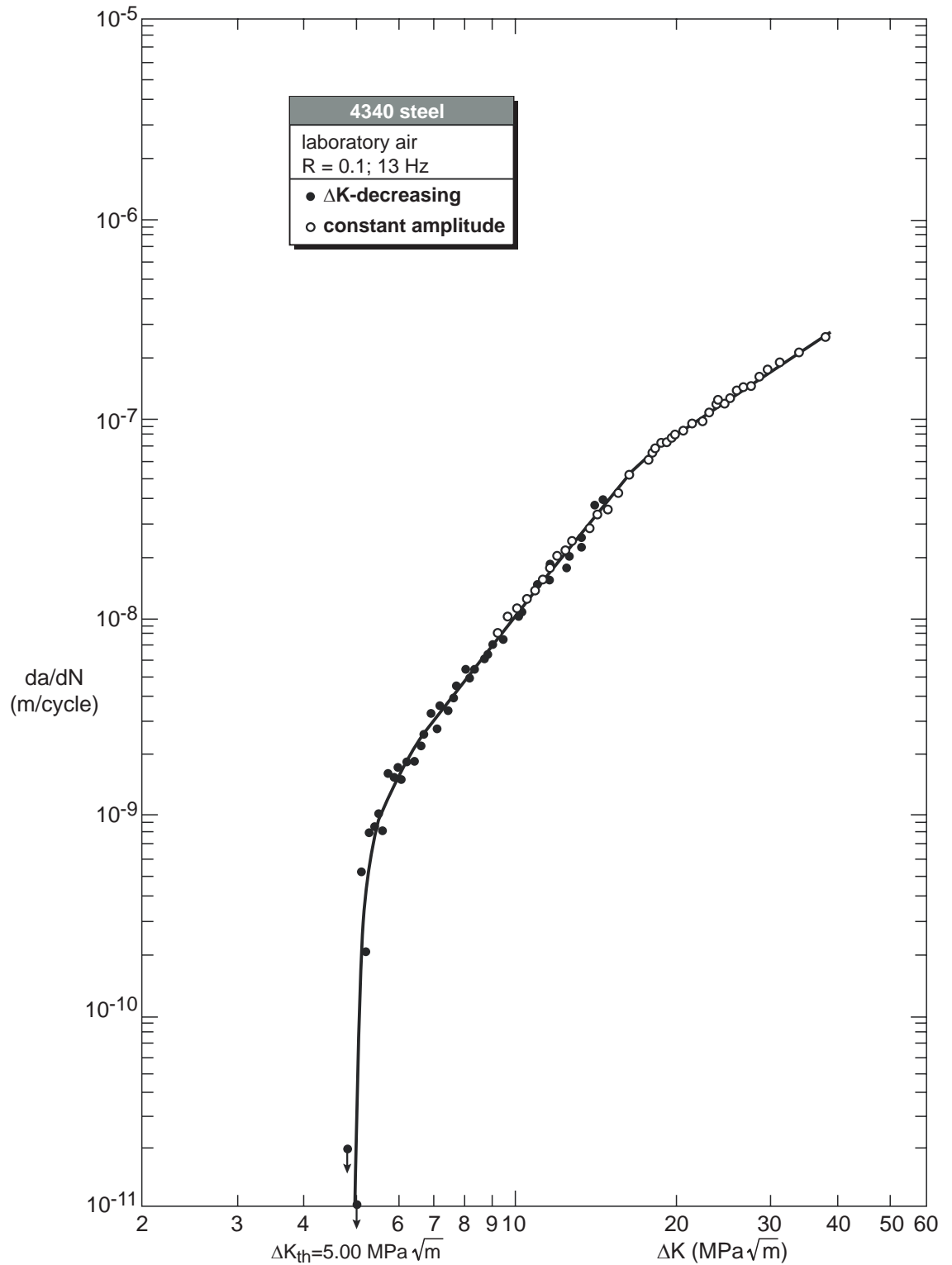


Fig. 16 Constant amplitude and ΔK -decreasing fatigue crack growth rates for 4340 steel at R = 0.1

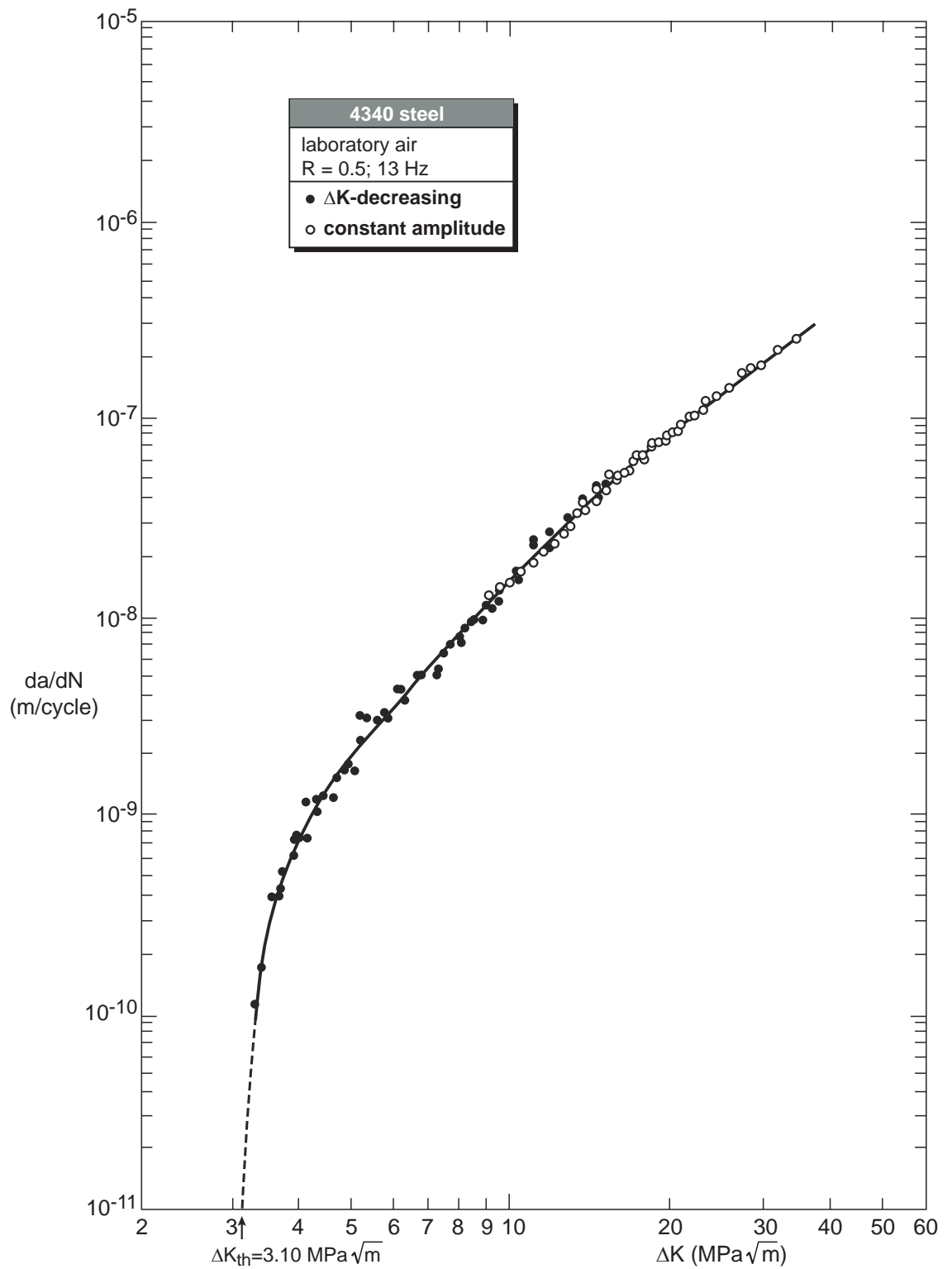


Fig. 17 Constant amplitude and ΔK -decreasing fatigue crack growth rates for 4340 steel at $R = 0.5$

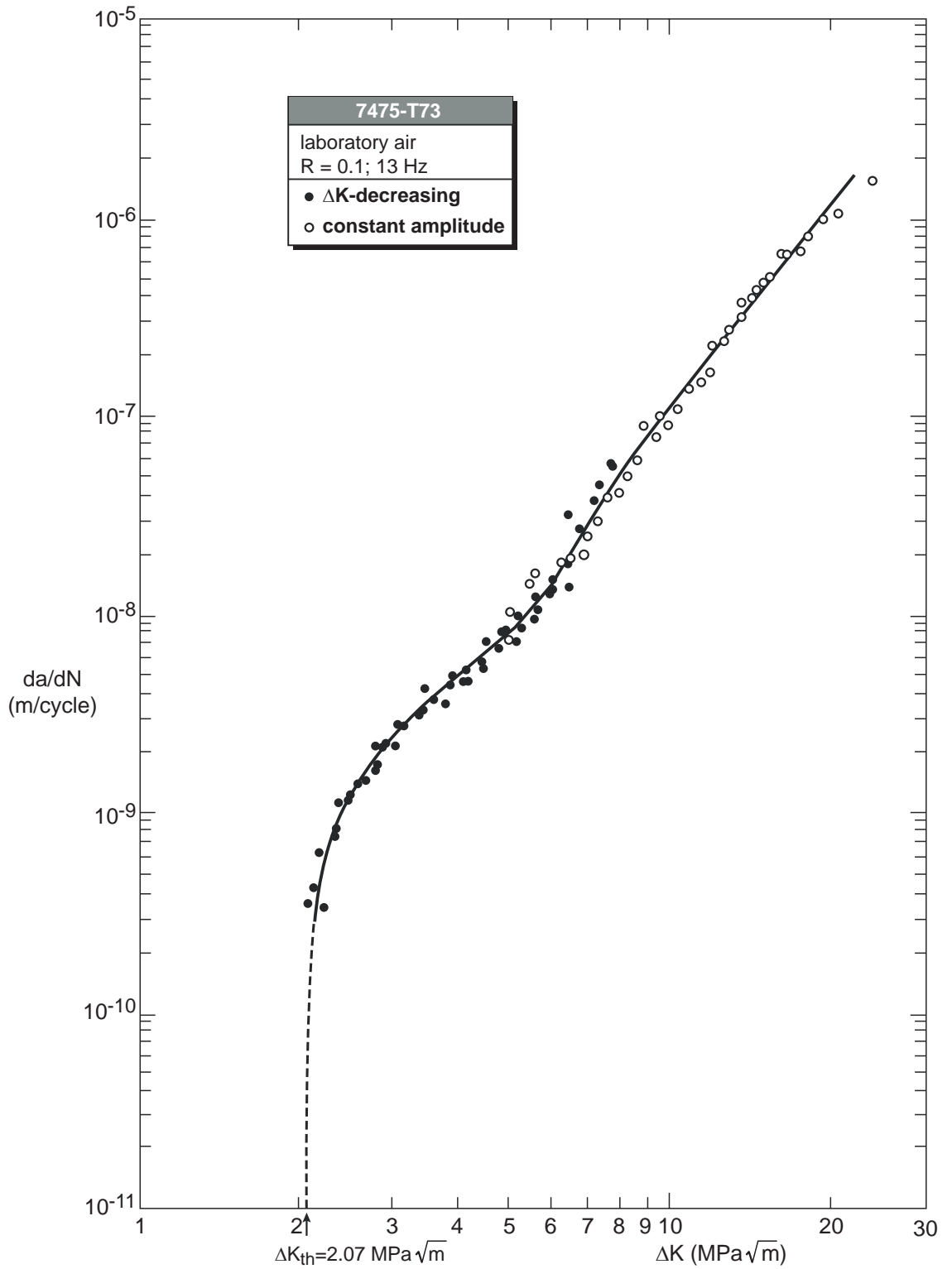


Fig. 18 Constant amplitude and ΔK -decreasing fatigue crack growth rates for 7475-T73 at $R = 0.1$

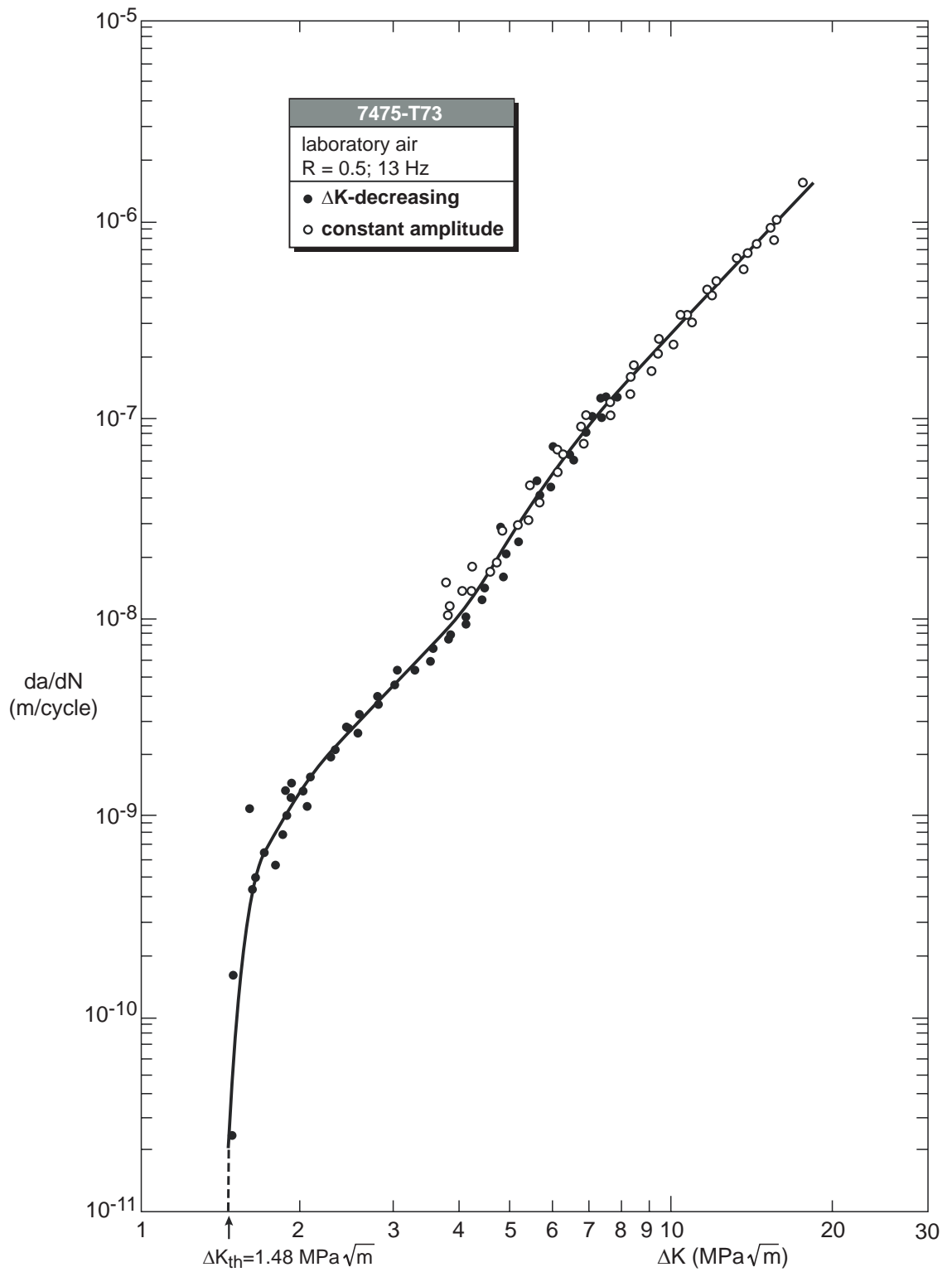


Fig. 19 Constant amplitude and ΔK -decreasing fatigue crack growth rates for 7475-T73 at $R = 0.5$

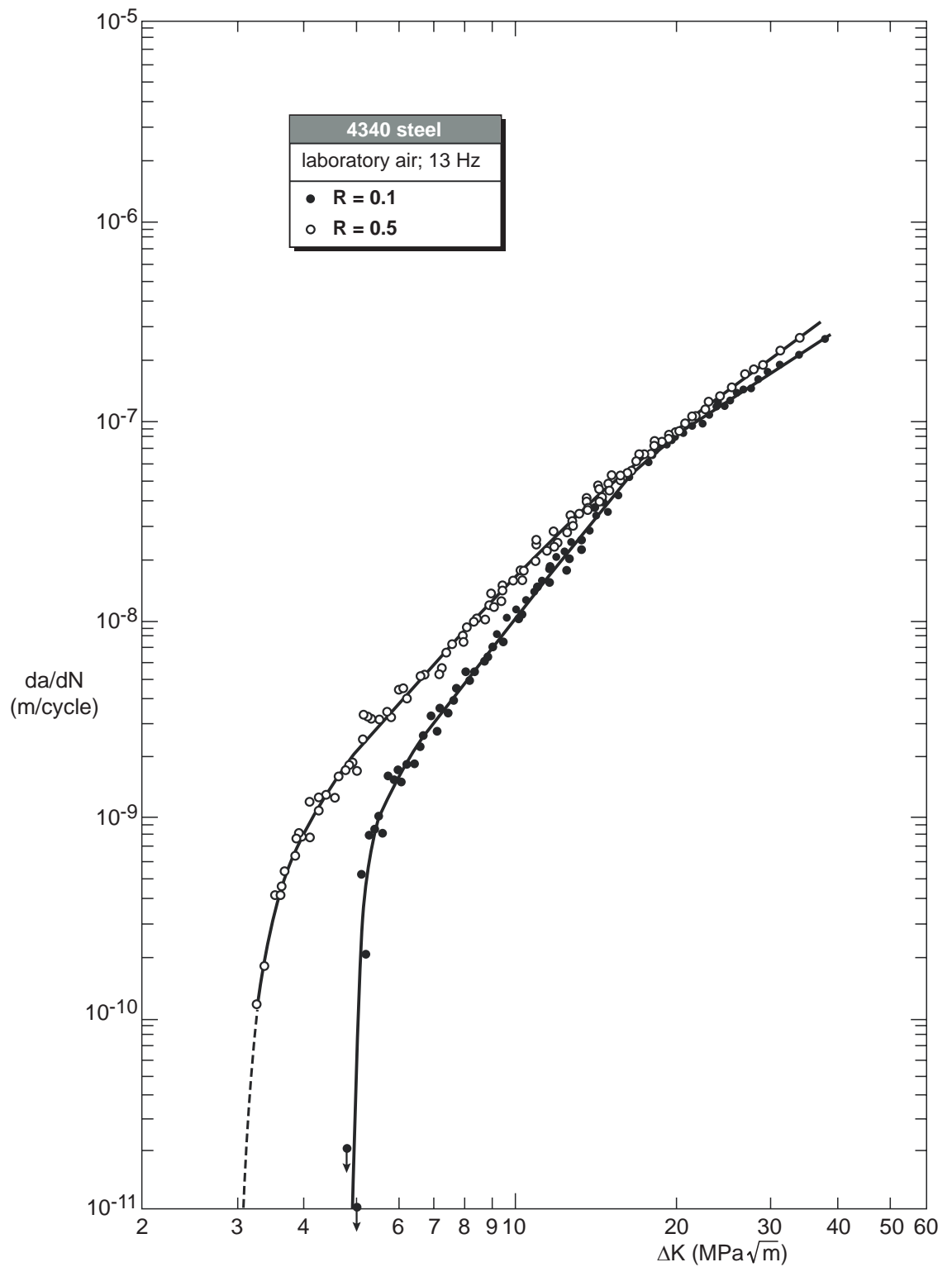


Fig. 20 Comparison of constant amplitude and ΔK -decreasing fatigue crack growth rates for 4340 steel at $R = 0.1$ and $R = 0.5$

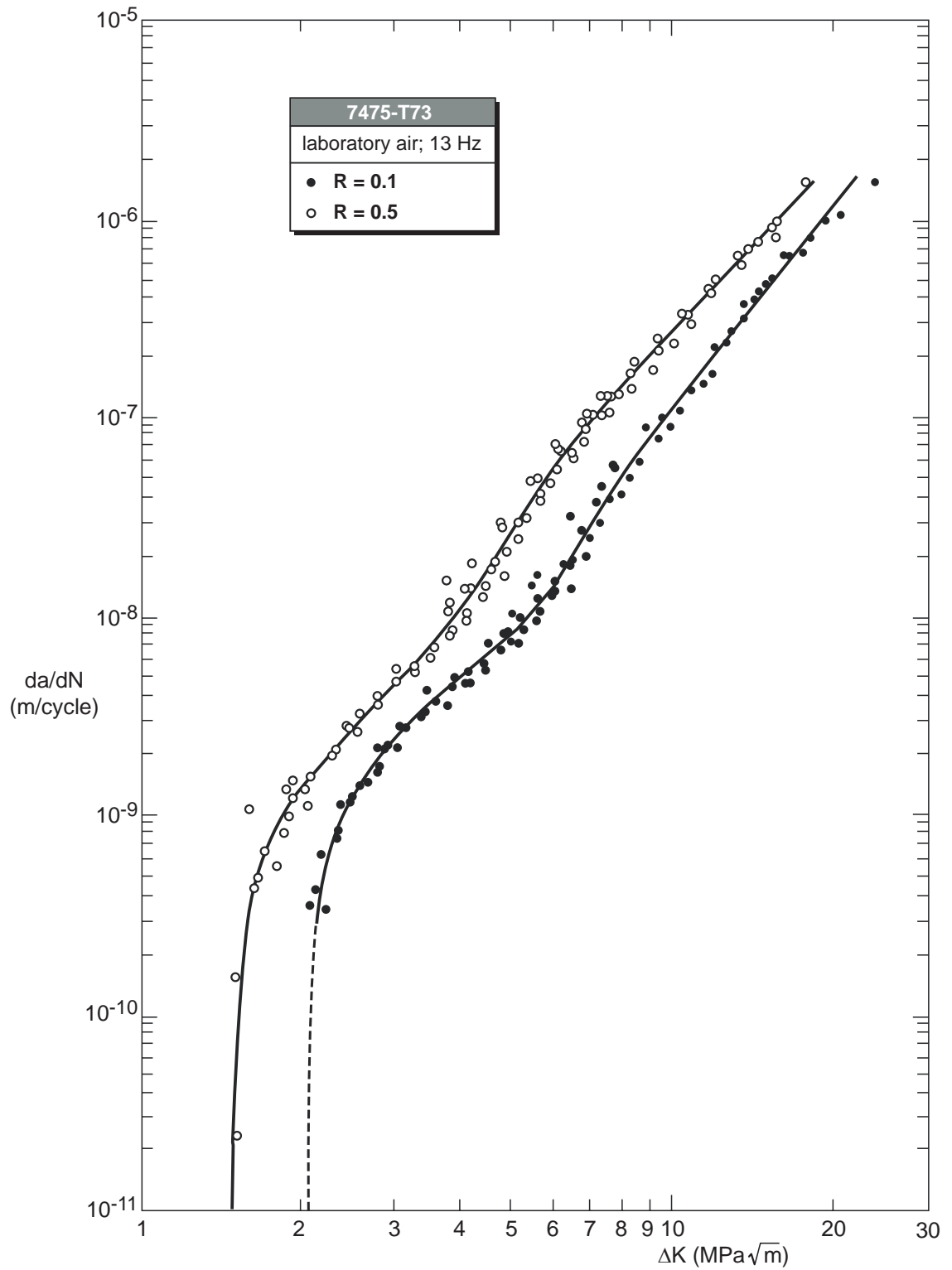


Fig. 21 Comparison of constant amplitude and ΔK -decreasing fatigue crack growth rates for 7475-T73 at $R = 0.1$ and $R = 0.5$

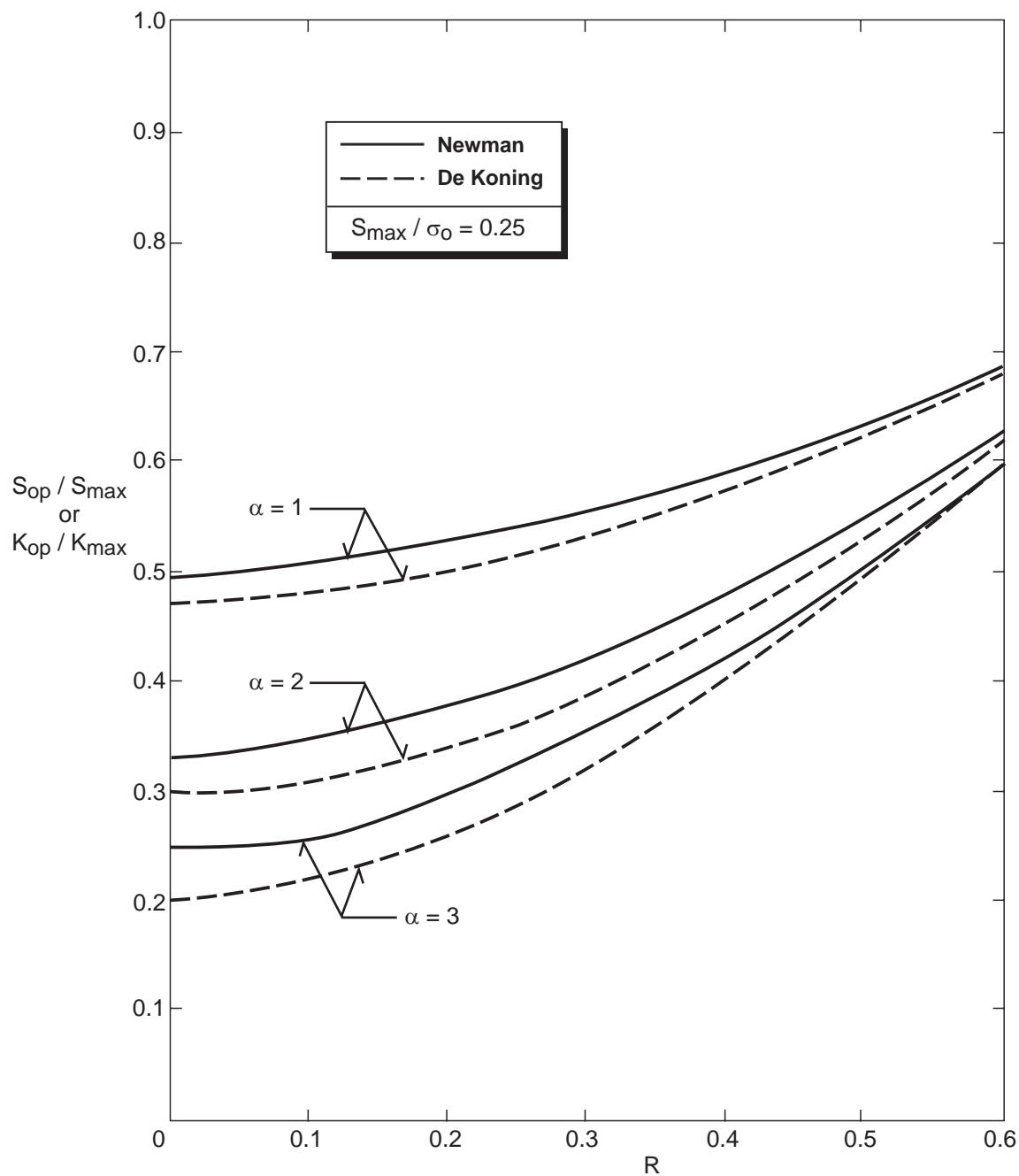


Fig. 22 Comparison of fatigue crack opening levels predicted by the models of Newman (1981) and De Koning and Liefing (1988)

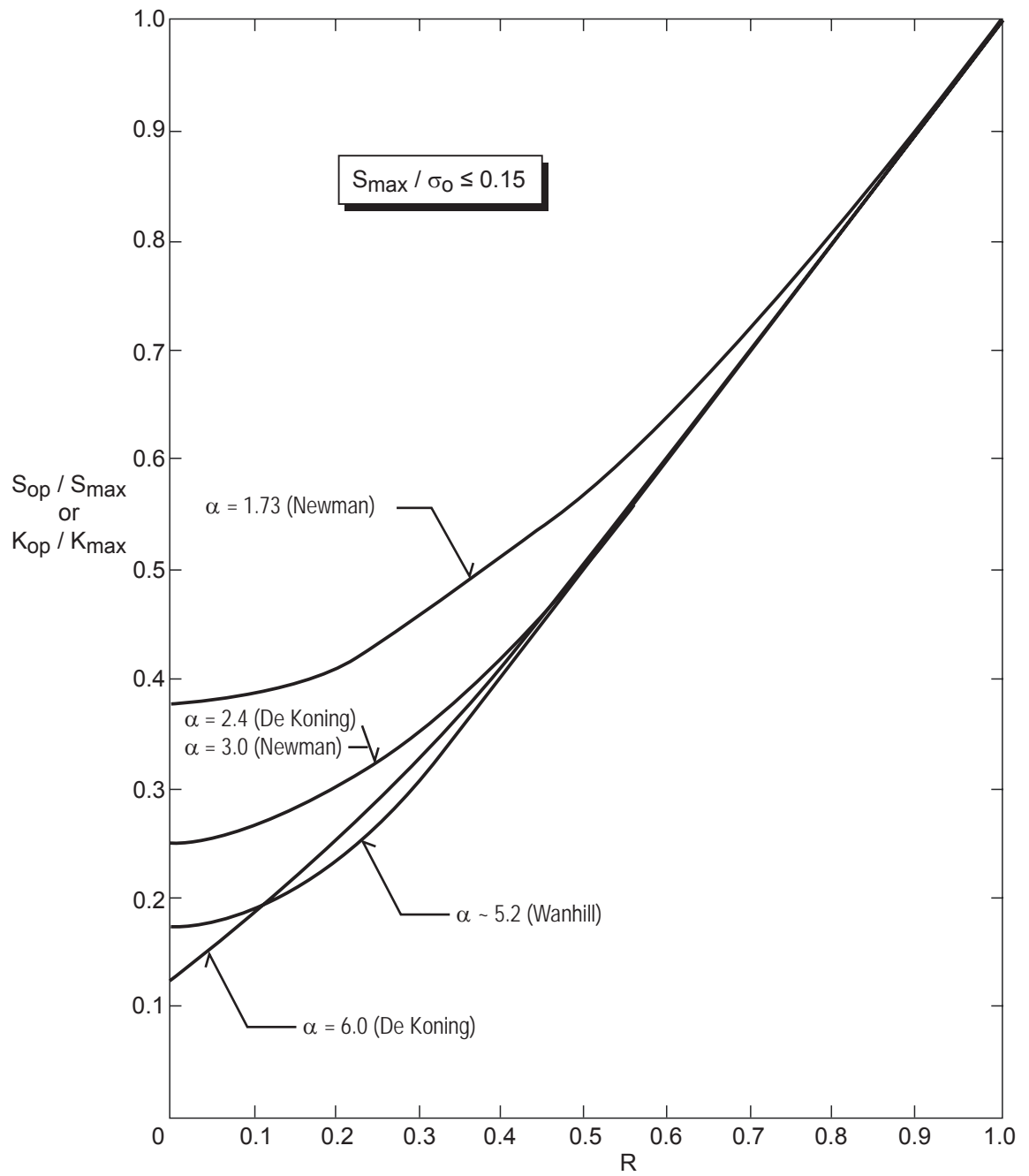


Fig. 23 Fatigue crack opening levels predicted by the models of Newman (1981) and De Koning and Liefing (1988) and derived from empirical equations for 4340 steel by Wanhill and De Koning

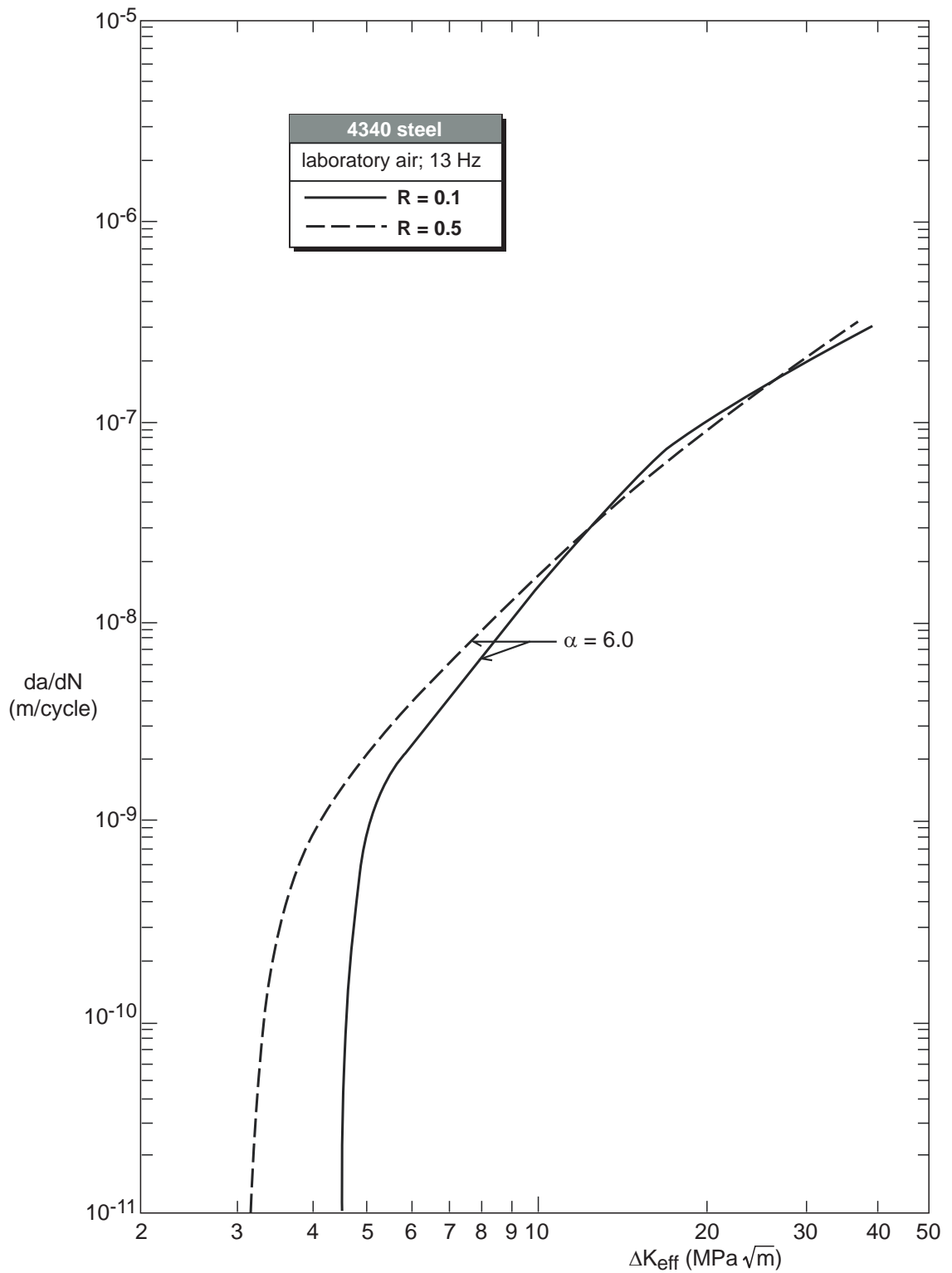


Fig. 24 Correlation of constant amplitude and ΔK -decreasing fatigue crack growth rates for 4340 steel by ΔK_{eff}

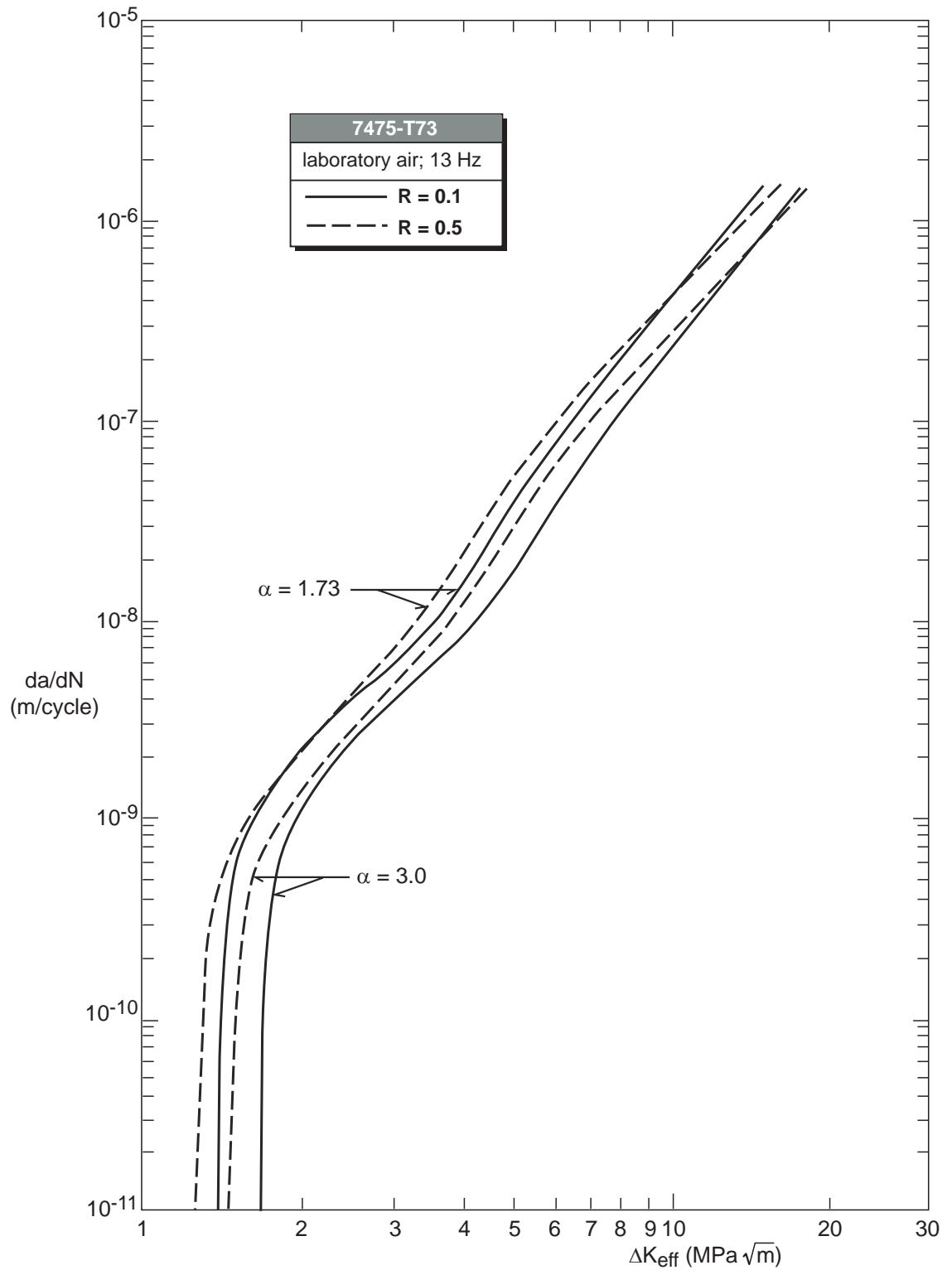


Fig. 25 Correlation of constant amplitude and ΔK -decreasing fatigue crack growth rates for 7475-T73 by ΔK_{eff}

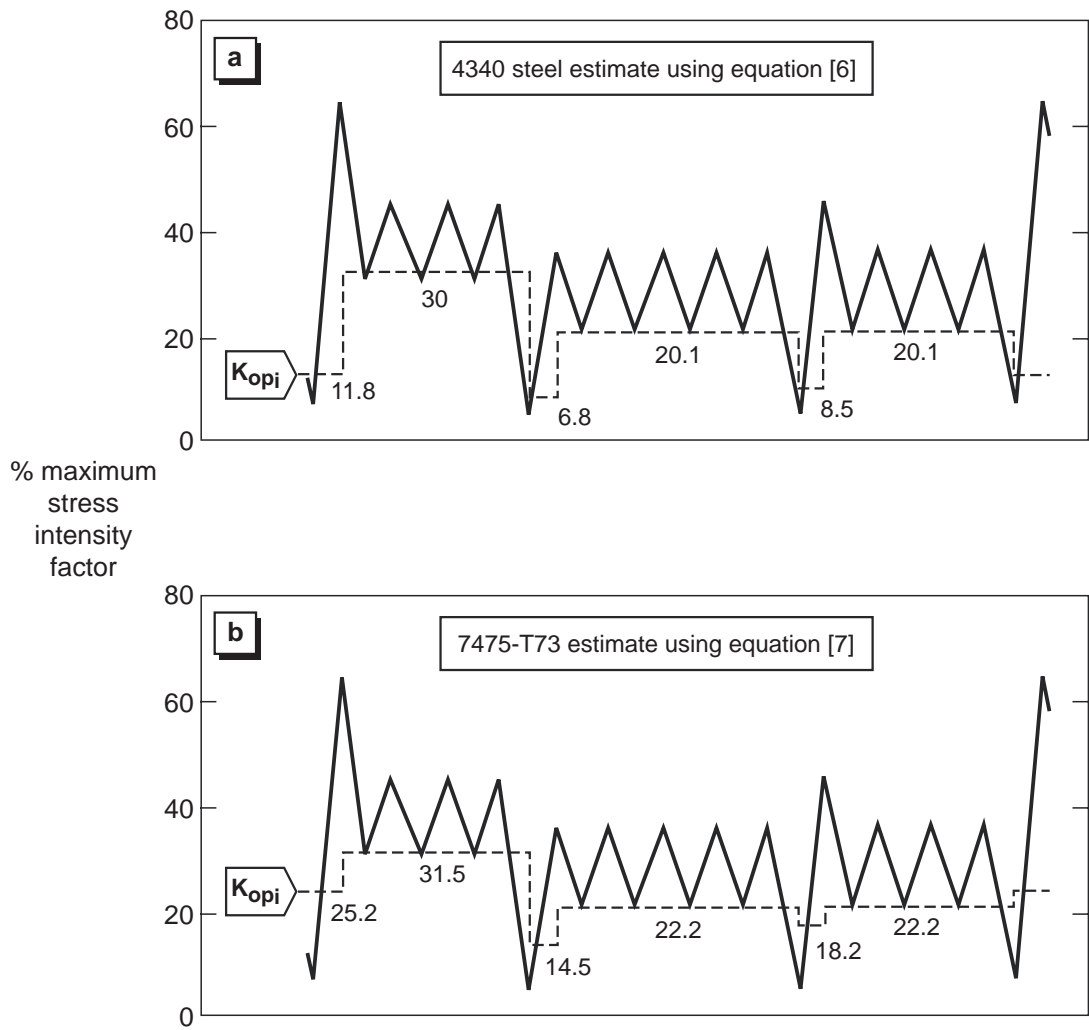


Fig. 26 Estimates of K_{Opi} during a flight block. Compare with figure 8

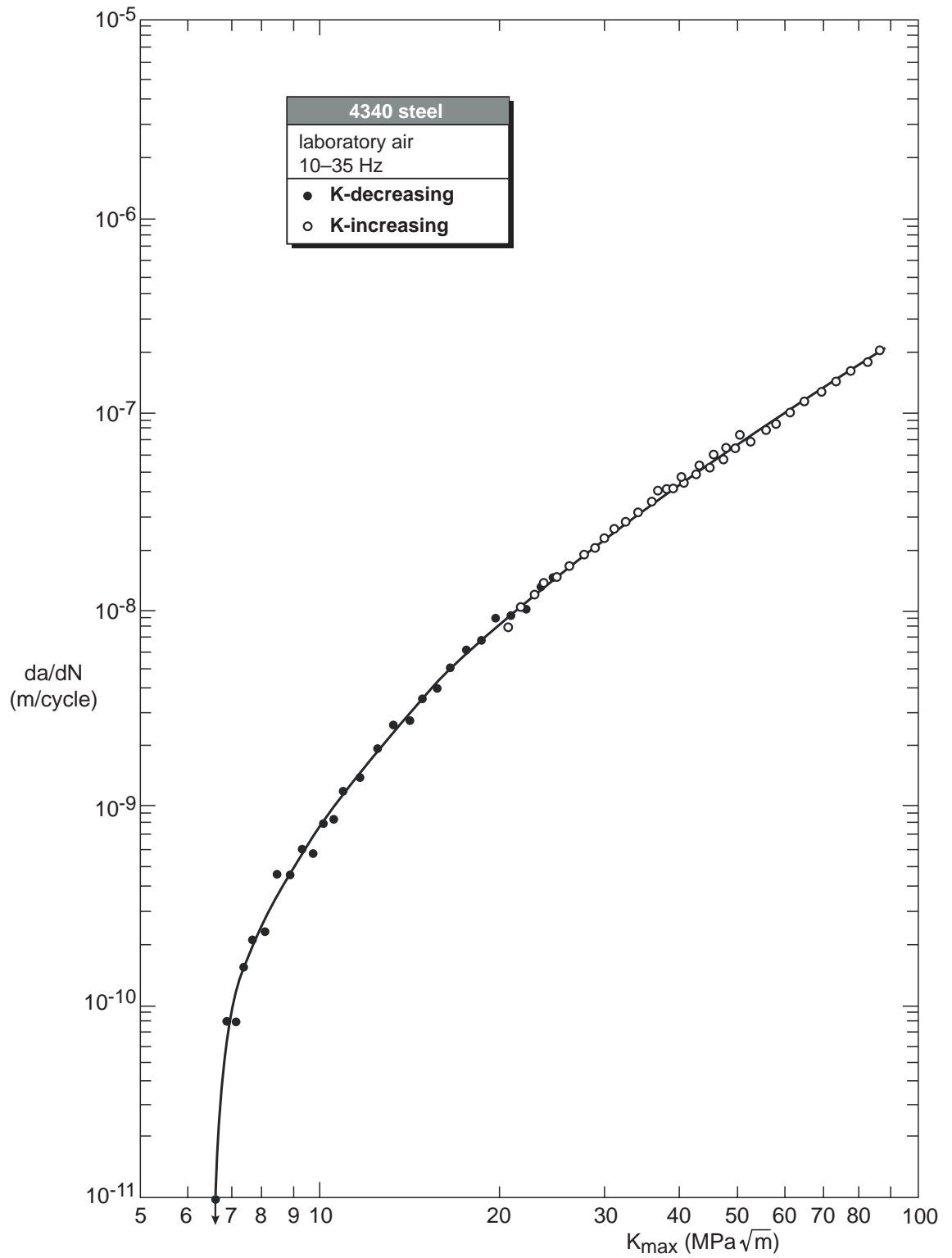


Fig. 27 Landing gear block programme fatigue crack growth rates for 4340 steel

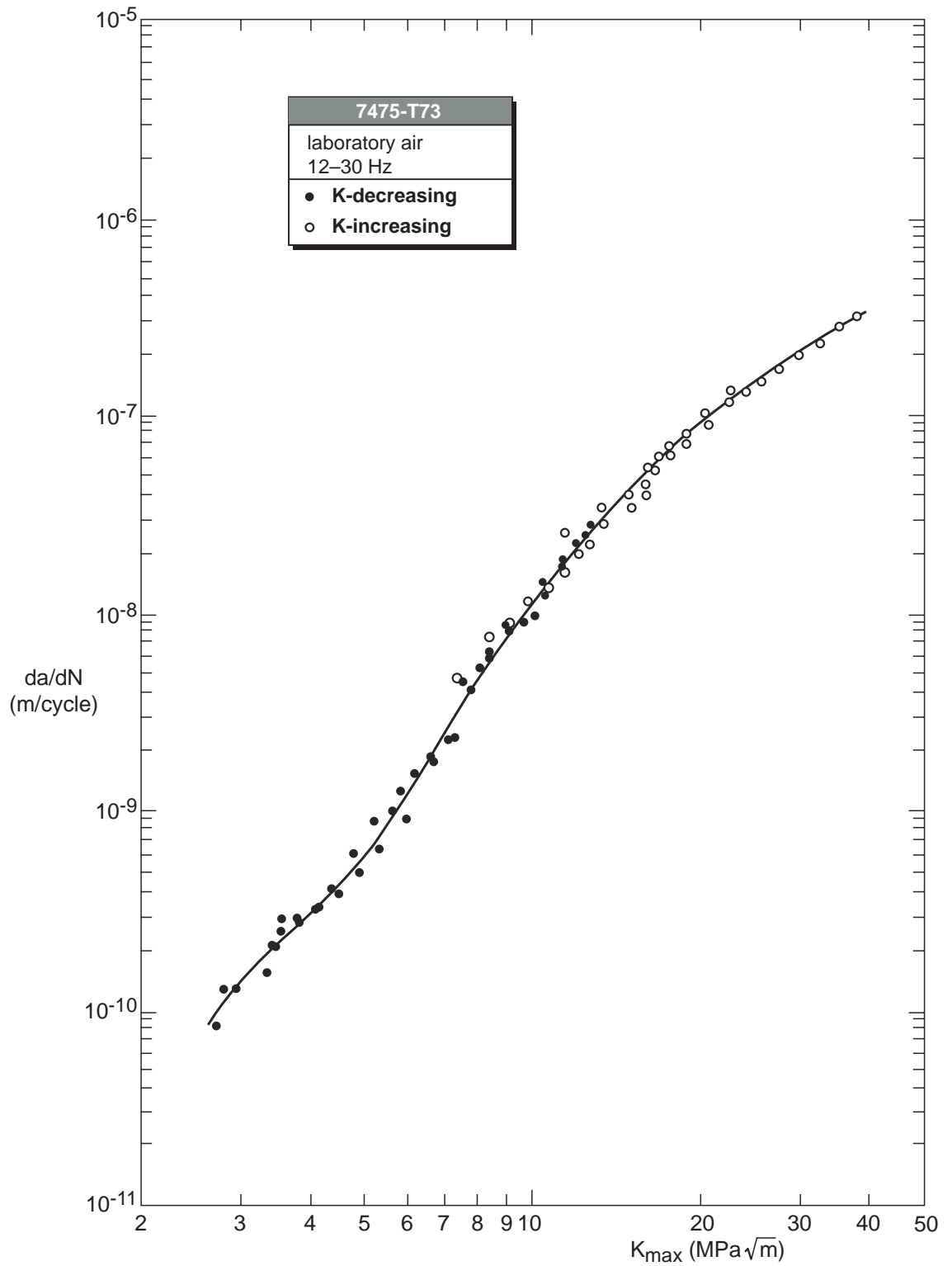


Fig. 28 Landing gear block programme fatigue crack growth rates for 7475-T73

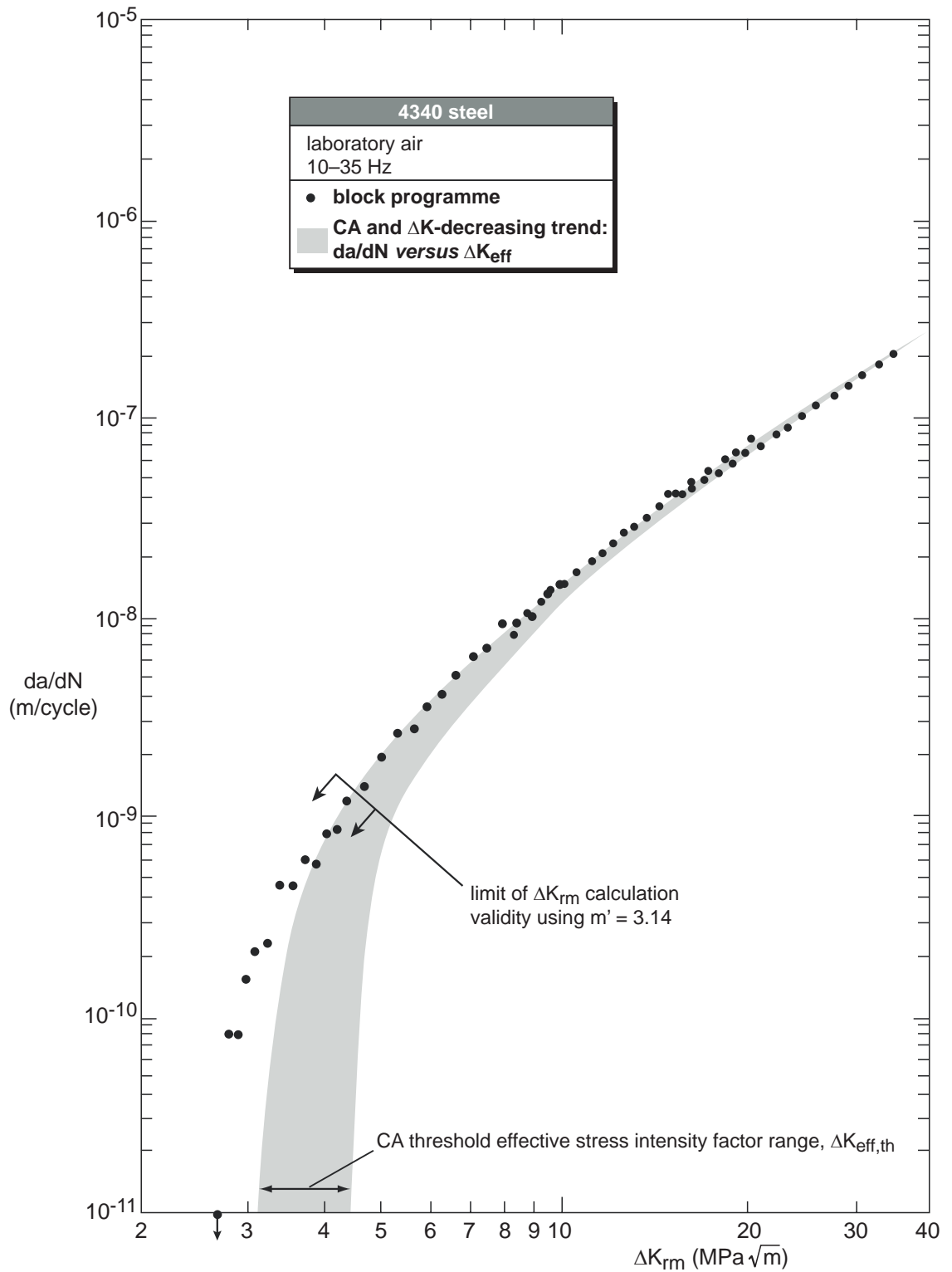


Fig. 29 Correlation of block programme and CA and ΔK -decreasing fatigue crack growth data for 4340 steel by ΔK_{rm}

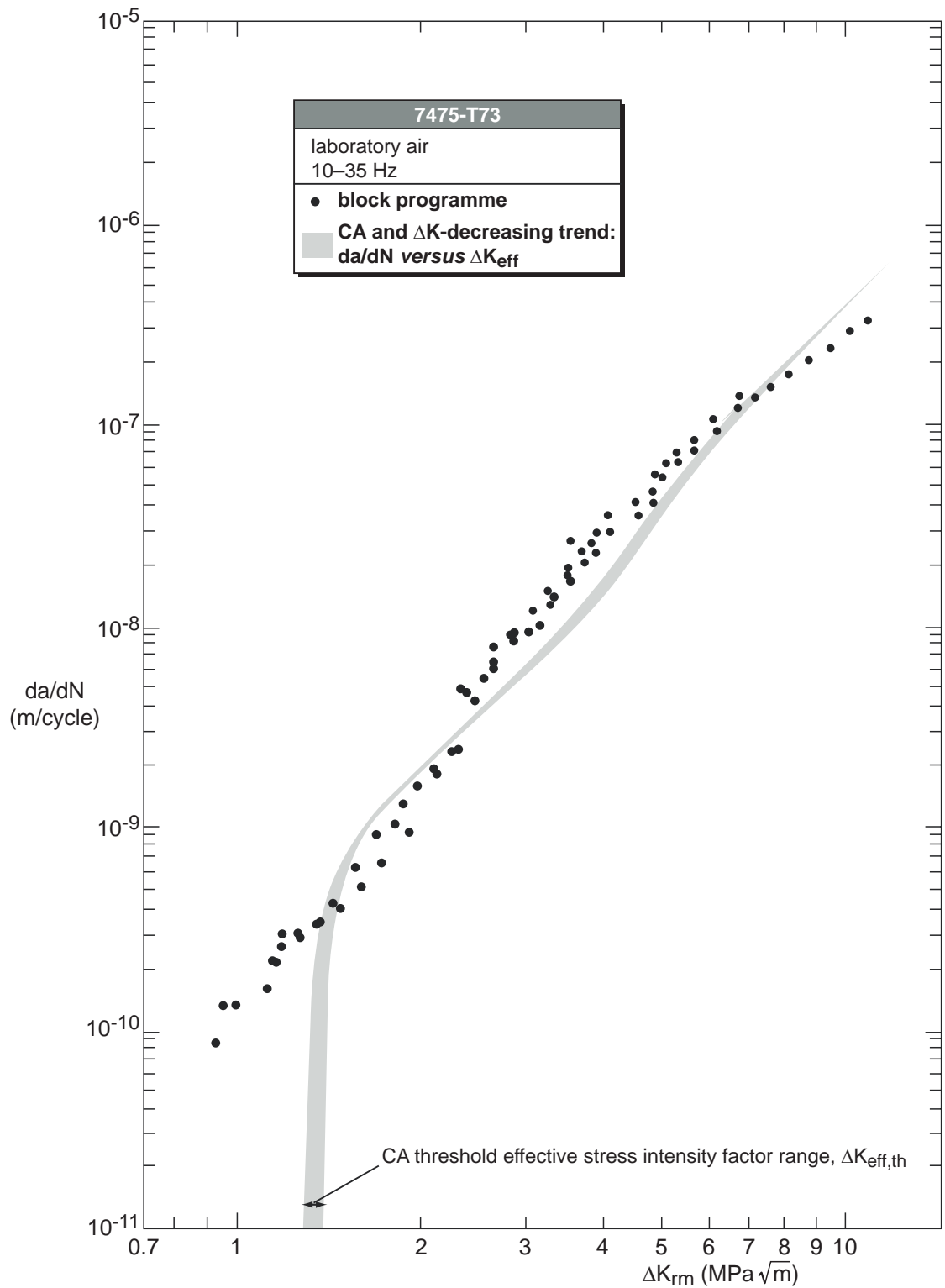


Fig. 30 Correlation of block programme and CA and ΔK -decreasing fatigue crack growth data for 7475-T73 by ΔK_{rm}

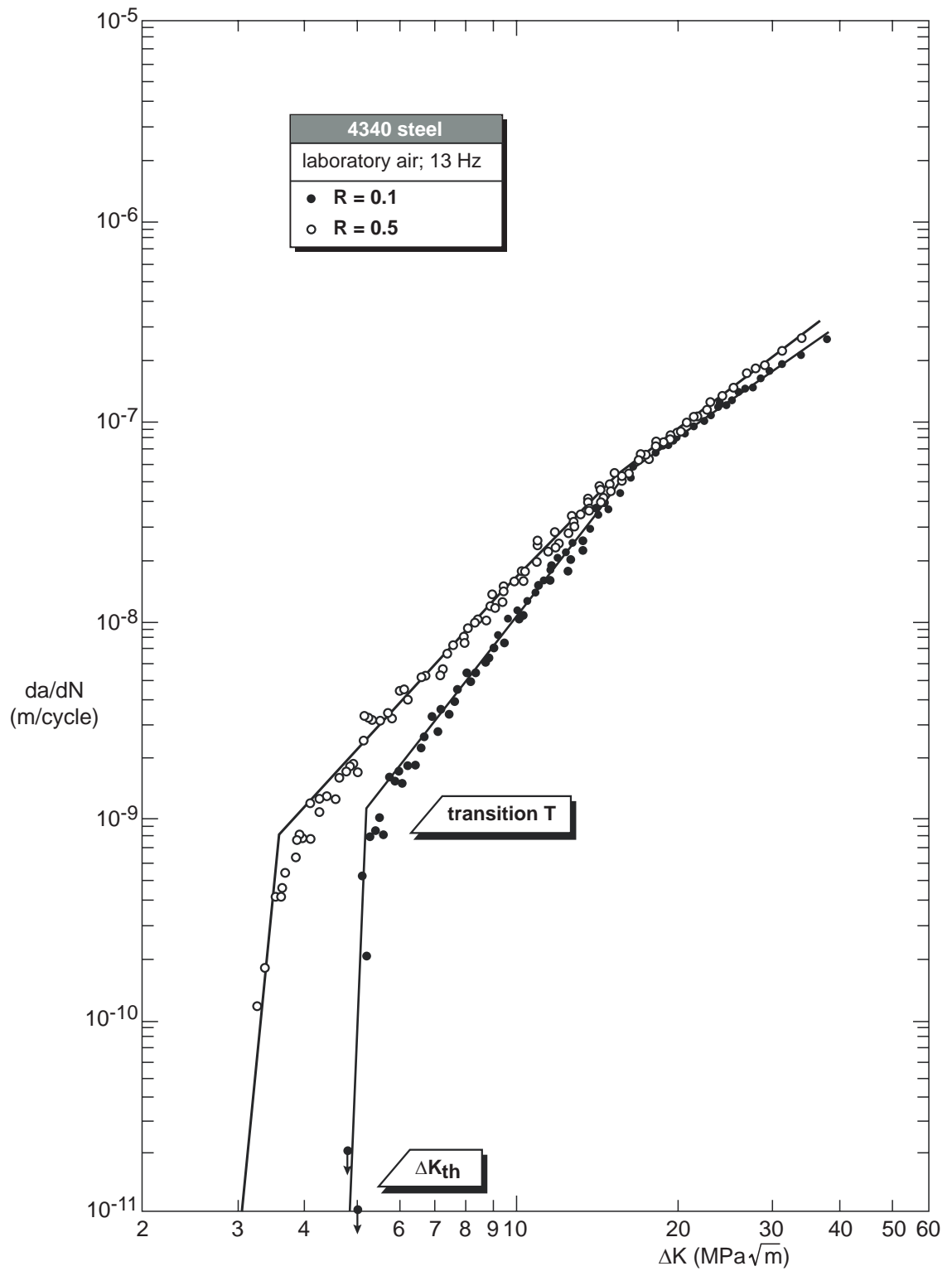


Fig. 31 Multi-linear approximations to the fatigue crack growth curves for 4340 steel tested under constant amplitude and ΔK -decreasing loading

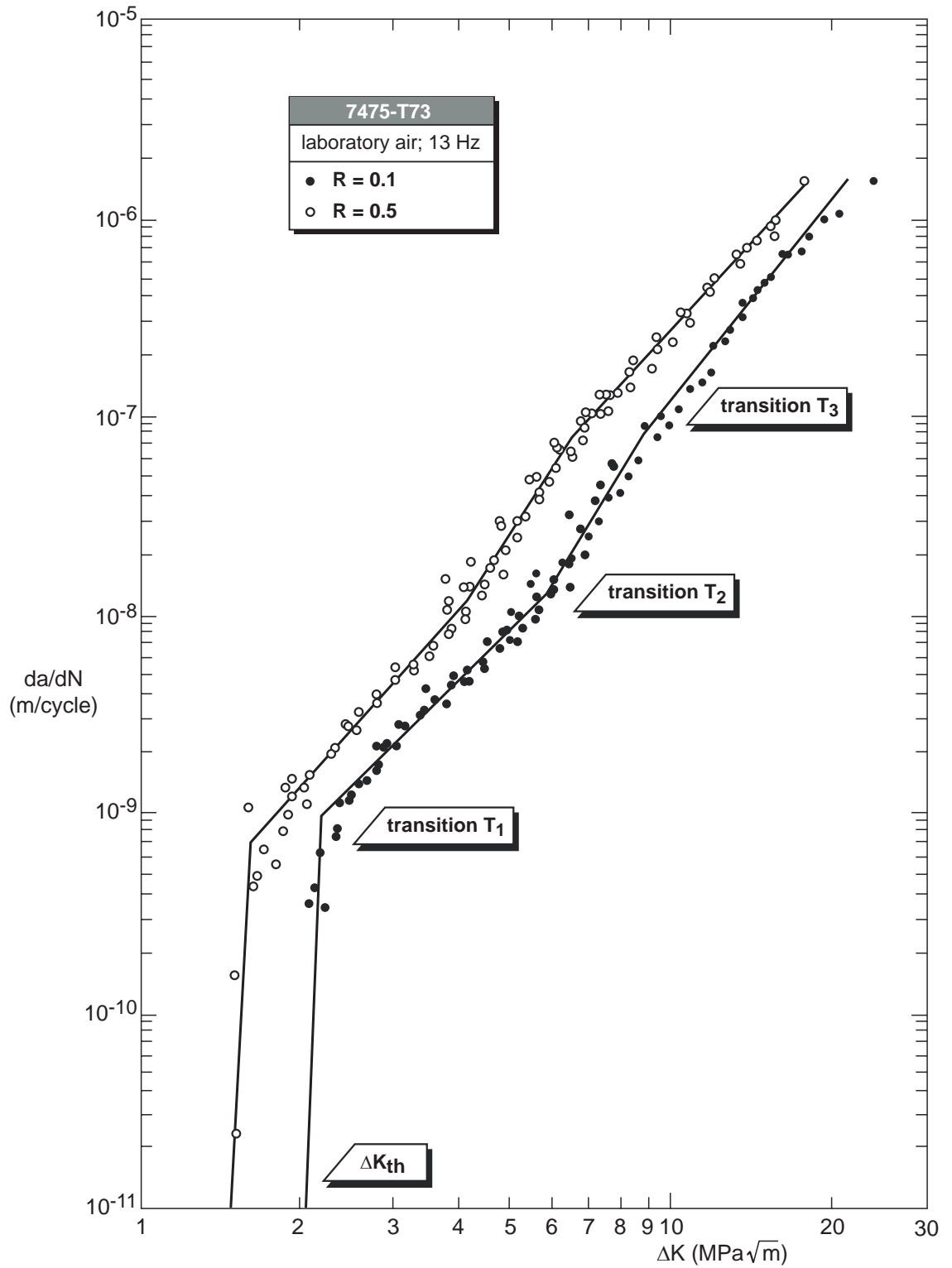


Fig. 32 Multi-linear approximations to the fatigue crack growth curves for 7475-T73 tested under constant amplitude and ΔK -decreasing loading

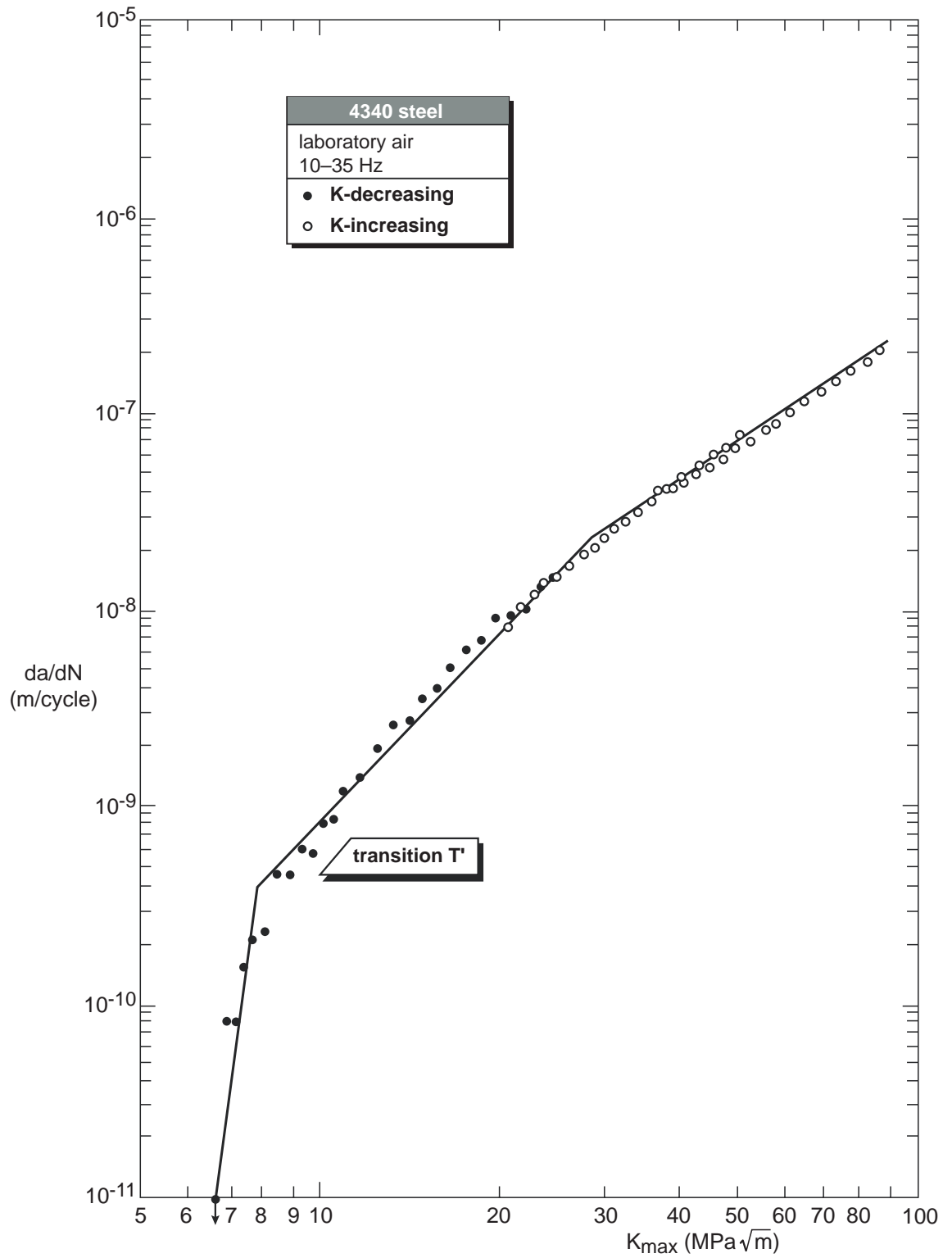


Fig. 33 Multi-linear approximations to the fatigue crack growth curves for 4340 steel tested under landing gear block programme loading

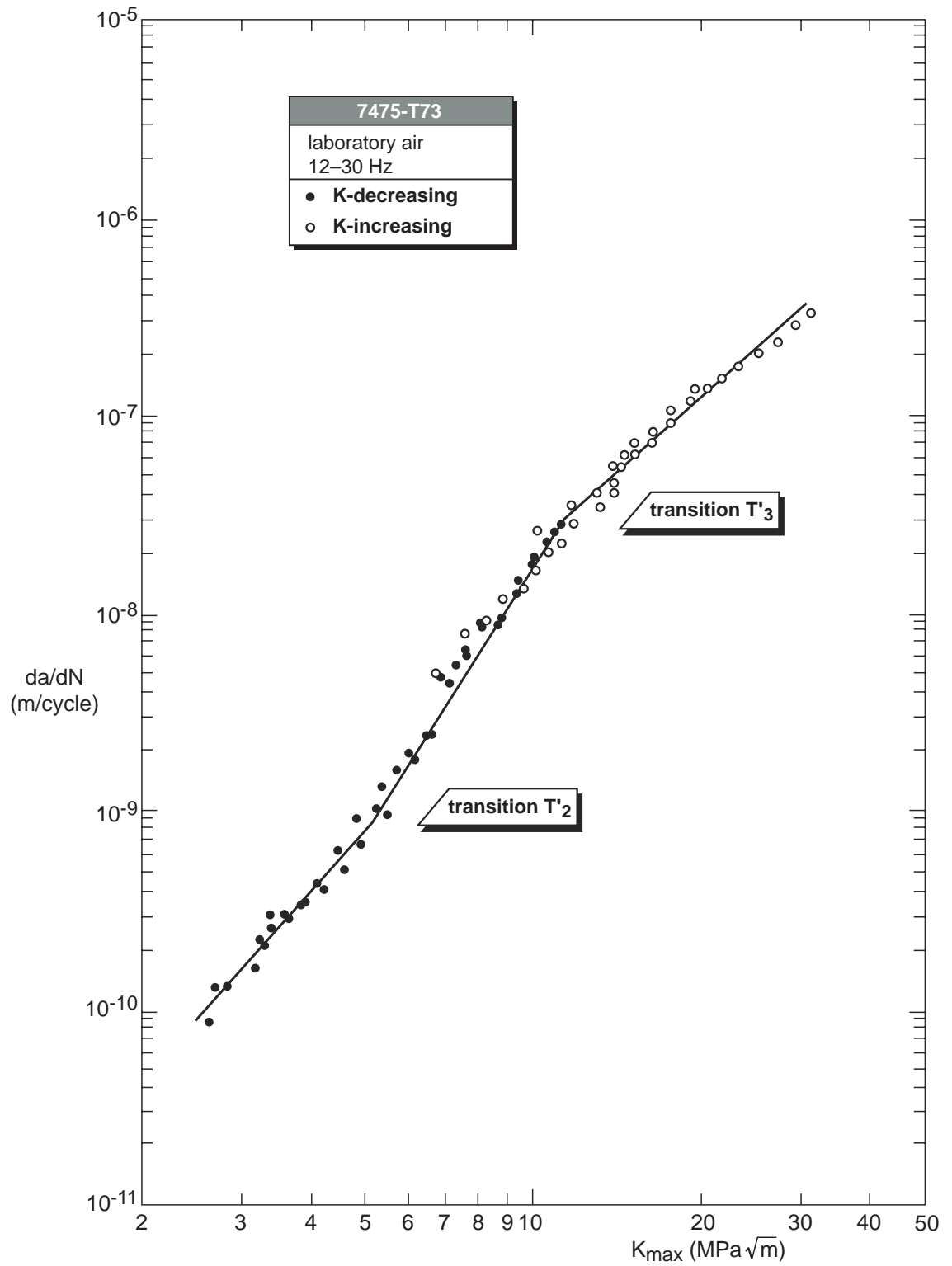


Fig. 34 Multi-linear approximations to the fatigue crack growth curves for 7475-T73 tested under landing gear block programme loading